ELASTIC AND INELASTIC SCATTERING OF PROTONS

FROM ^{6}Li BETWEEN 25 and 45 MeV

by

Giovanni LoBianco

A thesis submitted to the Department of Physics
of the University of Manitoba in partial fulfill-
ment of the requirements for the Degree of Master
of Science.

March 1970

ABSTRACT

Using the University of Manitoba sector-focussed cyclo-
tron a study has been made of the elastic and inelastic
scattering of protons from ^{6}Li. Data were obtained at
25.9, 29.9, 35.0, 40.1 and 45.4 MeV. The 2.18 MeV (3^+,
T = 0) state of ^{6}Li was found to be strongly excited, but
the 3.56 MeV (0^+, T=1) state was quite weakly excited.
To test the applicability of the optical model description
for the scattering from such a light nucleus the elastic
angular distributions have been analysed using the automatic
search code SEEK. Available polarization angular distribu-
tions were included in the analysis. Good fits have been
obtained for quite acceptable optical model parameters.
Angular distributions for excitation of the 2.18 MeV level
were measured at all five energies. Angular distributions
for excitation of the 3.56 MeV level were measured at 25.9
and 45.4 MeV. An analysis in terms of a microscopic theory
may give information about the spin-isospin dependent part of
the effective interaction.

ACKNOWLEDGMENTS

iii

CONTENTS

Page

LIST OF FIGURES

CHAPTER 1

1-1 Introduction

The present thesis describes an experiment in which protons

from the University of Manitoba sector focussed cyclotron were scatter-

ed by a ^{6}Li target. The incident protons had energies of 25.9, 29.9,

35.0, 40.1 and 45.4 MeV, and data were collected for elastic scattering

and for inelastic scattering from the first and second excited states of ^{6}Li.

The elastic scattering data have been analysed using the

optical model. An analysis of the inelastic scattering from the 3.564

MeV (0^+, T=1) level in ^{6}Li is planned for the near future according

to a microscopic description of the interaction. It is suggested that

the angular distributions corresponding to the 2.184 MeV (3^+, T=0) state

in ^{6}Li would form an interesting subject for a copuled channels calculation.

It is the intention to examine in the first chapter in some

detail the purpose of the experiment and the motives for a theoretical

analysis of the data obtained, and to give an account of related investi-

gations which have appeared in the literature. The main part of the dis-

cussion is contained in section 4, while the two preceeding sections

are intended as a review of some of the basic material involved; sec-

tion 2 contains an account of the fundamentals of the nuclear optical

model, while section 3 deals with the present knowledge and understanding

of the features of the ^{6}Li spectrum. The second chapter contains a des-

cription of the experimental arrangement and of the methods followed in

the reduction of the experimental data. In the third and final chapter

the results obtained are presented and discussed. Appendix I contains

the derivation of a few formulas used in the data reduction. Finally,

tables of the differential cross-sections are given in appendix II.

1-2. The Optical Model

A comprehensive presentation of the optical model theory is

outside the scope of this thesis and can be found for instance, in

monographs written by Hodgson {1} and by Jones {2}. We shall limit our-

selves to an account of the basic ideas together with a sketch of the

historical development. Around 1950 the interaction of a neutron with

a nucleus was thought to correspond to the following picture:

1) At very low energies (keV range), where the only channels

open are elastic scattering and radiative capture, the dependence on energy

of the differential and total cross-sections shows strongly peaked reson-

ances. The scattering cross-section is the sum of terms corresponding

to two different processes. The first (potential scattering) is a sur-

face phenomenon in which the nucleus behaves as a hard sphere, while

the second corresponds to the capture of the neutron to form a compound

nucleus, which decays after a time of $\sim 10^{-14}$ seconds. The compound scat-

tering is responsible for the resonances: the neutron can be absorbed

only at those energies at which the wave function of the incident neutron

at the nuclear surface satisfies the boundary conditions appropriate for

the wave function describing a neutron inside the compound nucleus. At

all other energies the nuclear surface is perfectly reflecting (resonance

scattering). The mathematical formulation of these ideas leads to
the famous Breit-Wigner resonance formulas. {3}

2) At higher energies ($\gtrsim$8MeV) the number of channels avail-
able for the decay of the compound nucleus becomes so great that the
probability of decay through the entrance channel is negligible. At
the same time the separation between two adjoining states of the compound
nucleus becomes less than their width. As a consequence the scattering
is potential scattering. As the energy of the incident neutrons increases,
the scattering cross-section remains constant while the reaction cross-
section decreases regularly, being inversely proportional to the velocity.

In conclusion, at energies where the continuum theory is appli-
cable, the total cross-section is expected to decrease smoothly with
increasing incident energy. The same is expected to happen at lower
energies for the "gross" variation of the cross-section, which is obtain-
ed by averaging over the resonances.

At the beginning of the fifties this picture was partially con-
tradicted by experimental observations. On one hand, experiments like the
one of Eisberg and Igo {4} (inelastic proton scattering at 32 MeV) gave
strongly forward peaked angular distributions and relatively large values
of the (p,p') cross-section while the compound nucleus theory predicts
angular distributions symmetric about 90° and strongly favours the (p,n)
process over the (p,p') process. On the other hand, evidence of phenomena
that could not be explained in terms of the compound theory was given by
the discovery of the giant resonances (Barschall {5}): plots of the total
cross-section versus energy show broad peaks (of width ~1 MeV) whose posi-

tion and height vary regularly with the mass number of the target. This behaviour can be explained if one supposes that the nucleus, instead of being perfectly reflecting away from resonances, is partially absorbing. The potential scattering is then no more hard sphere scattering, the incident wave function penetrates into the nuclear well, and a resonance is produced when this can accomodate an integer number of half wavelengths.

From a mathematical point of view the partial absorption of the incident wave function can be obtained if one represents the nucleus by a complex potential well (optical potential). To illustrate this point, and to indicate how the cross-sections can be calculated, we shall consider the very simple case of $\ell=o$ neutrons and of a complex potential of the square well type:

$$V(\underline{r}) = -V-iW, \qquad r < R$$
$$= 0 \qquad r > R$$

Let us recall some well known formulas relative to the scattering of a plane wave by a central potential of range R. The asympotic solution of the Schrödinger equation, the differential cross-section for elastic scattering and the scattering cross-section are given by:

$$(1) \quad \psi(\underline{r}) = \frac{\sqrt{\pi}}{kr} \sum_{\ell=o}^{\infty} \sqrt{2\ell+1} \; i^{\ell+1} \left(e^{-i(kr-\frac{\ell\pi}{2})} - \eta_\ell e^{i(kr-\frac{\ell\pi}{2})} \right) Y_{\ell o}$$

$$(2) \quad \frac{d\sigma_{e\ell}}{d\Omega} = \frac{\pi}{k^2} \left| \sum_{\ell=o}^{\infty} \sqrt{2\ell+1} \; (1-\eta_\ell) \; Y_{\ell o} \right|^2$$

(3) $\quad \sigma_{e\ell} = \frac{\pi}{k^2} \sum_{\ell=0}^{\infty} (2\ell+1) \; |1-n_\ell|^2 \; ;$

where $n_\ell = e^{i2\delta}\ell$ and the phase shifts δ_ℓ are obtained by imposing the continuity of the radial wave function and of its derivative at the boundary $r \dot= R$.

In our case the radial solution is:

$$u = A(\sin \sqrt{\frac{2m}{\hbar^2} (E+V+iW)} \; r) \qquad , \qquad r \quad <R$$

$$\quad = B \sin(\sqrt{\frac{2mE}{\hbar^2}} \; r + \delta o) \qquad , \qquad r \quad >R$$

and the continuity condition:

$$\sqrt{\frac{2m}{\hbar^2} (E+V+iW)} \;\; \cotg \;\; \sqrt{\frac{2m}{\hbar^2} (E+V+iW)} \; R_F \; \sqrt{\frac{2mE}{\hbar^2}} \;\; \cotg \; (\sqrt{\frac{2mE}{\hbar^2}} R + \delta o}$$

gives a complex phase shift δ_0, so that $|\eta_0|<1$. As a consequence the amplitude of the outgoing wave (second term in the asympotic solution {1}) is less than the amplitude of the incoming wave, the difference being proportional to the number of particles absorbed per unit time. The same method gives the complex phase shifts in the case of any ℓ and different shapes of the potential, but, of course, the integration of the radial wave equation becomes in general far from trivial and numerical methods have to be employed.

Substitution of the phase shifts in the general formulas (2) and (3) gives the differential cross-section and the scattering cross-section while the reaction (absorption) and total cross-section are given by:

$$(4) \quad \sigma_{re} = \frac{\pi}{k^2} \sum_{\ell=o}^{\infty} (2\ell+1) \, (1-|\eta_\ell|^2)$$

$$(5) \quad \sigma_{tot} = \sigma_{el} + \sigma_{re} = \frac{\pi}{k^2} \sum_{\ell=o}^{\infty} (2\ell+1) \, 2 \, \mathrm{Re} \, (1-\eta_\ell)$$

It should be noted that the optical model does not contradict the idea of the formation of a compound nucleus, but only the assumption of perfect reflection away from resonances. Actually at low energies the optical model and the compound nucleus theory are complementary, the former giving the general trend of the dependence of the total cross-section on the incident energy, the latter giving the details of this dependence.

At energies corresponding to the continuum, the optical model gives the cross-section for the formation of the compound nucleus, while its decay in one or another of the available channels, given the great number of these, can be treated from a statistical point of view (statistical theory). At these energies, however, the formation of the compound nucleus is not the only possible reaction mechanism, and, in particular, reactions involving charged particles, where emission from the compound nucleus is inhibited by the Coulomb barrier, follow generally the direct-reaction pattern.

In earlier studies of the optical model, like the one by Feshbach, Porter and Weisskoff {6}, a square well potential was used. It was found however, that a better agreement with experiment is obtained using a potential of the Woods-Saxon {7} type:

$$(6) \quad U(r) = \frac{-v-iW}{1+\exp\left|\frac{r-R}{a}\right|}$$

characterized by the four parameters, V. W. R, and a. V and W are
the strengths of the real and imaginary part of the potential, R is
the nuclear radius expressed in terms of the radius parameter r_0 and
of the atomic number by $R = r_0 A^{1/3}$, and a is the diffuseness parameter.
Generally better agreement with the experimental data is obtained when
the values of r_0 and a for the real and imaginary parts are different.

An improvement is obtained considering, together with the
volume absorption term (imaginary part of (6)), a surface absorption term,
of the form $+4iW_D a_D \frac{d}{dr} \left(\frac{1}{1+\exp\left|\frac{r-r_D A^{1/3}}{a_D}\right|}\right)$ (derivative Wood-Saxon form).

The reason for including this term is the following. The absorption pro-
cess is due to the collisions of the incident neutrons with the nucleons
of the target nucleus. Such collisions are opposed by the exclusion prin-
ciple, particularly in the inside of the nucleus, where most shells are
filled. So we expect the absorption to take place in preference at the
surface of the nucleus, especially at lower energies, where the exclusion
principle is more effective.

A further refinement of the optical potential is obtained with
the inclusion of a spin-orbit term, which accounts for the polarization
of the scattered particles. In analogy to the shell model potential,
the spin-orbit term is chosen to be of the Thomas form. An absorption
part in the spin-orbit term is sometimes included; however,
its utility is doubtful, except at very high energies. Also, when

the optical model is applied to the scattering of charged particles, a Coulomb term V_c must be included in the potential.

Taking into account the additional terms discussed, we obtain what we shall call the "standard form" of the optical potential.

$$(7) \quad U(r) = V_c(r) - \frac{V}{1+\exp\left(\dfrac{r-r_o A^{1/3}}{a}\right)} - \frac{iW}{1+\exp\left(\dfrac{r-r_w A^{1/3}}{a_w}\right)}$$

$$+ 4iW_D a_D \frac{d}{dr}\left(\frac{1}{1+\exp\left(\dfrac{r-r_D A^{1/3}}{a_D}\right)}\right) + (V_s+iW_s)\frac{4}{r}\frac{d}{dr}\left(\frac{1}{1+\exp\left(\dfrac{r-r_s A^{1/3}}{a_s}\right)}\right)(\underline{s}.\underline{\ell}.)$$

The potential (7) has been used extensively in the analysis of experimental data consisting of differential cross-section and polarization and total reaction cross-sections for a wide range of projectiles and target nuclei, at energies from a few MeV's to 150 MeV and over.

To fit, say, a differential cross-section angular distribution, the differential cross-sections are computed for all the angles considered using the potential (7) with a suitable set of starting parameters. Then the parameters are varied in order to minimize the quantity.

$$(8) \quad \chi^2 = \sum_{\substack{all \\ angles}} \left[\frac{\left(\dfrac{d\sigma}{d\Omega}\right)_{th} - \left(\dfrac{d\sigma}{d\Omega}\right)_{exp}}{\Delta\left(\dfrac{d\sigma}{d\Omega}\right)}\right]^2 \quad ,$$

where $\left(\dfrac{d\sigma}{d\Omega}\right)_{th}$ and $\left(\dfrac{d\sigma}{d\Omega}\right)_{exp}$ are the theoretical and experimental values of the differential cross-section and $\Delta\left(\dfrac{d\sigma}{d\Omega}\right)$ is the experimental error.

The optical model potential (7) contains thirteen adjustable

parameters and usually some additional condition is imposed in order to reduce this number. For example, it is quite common to set either W=0 (only surface absorption) or $W_D=0$ (only volume absorption), and when both terms are considered it is usual to take $r_W=r_D$.

The parameters, which give the best fit vary with type and energy of the projectile and with the atomic number of the target nucleus. Systematic optical model studies in progress in various laboratories have the purpose of finding the general trends in the variation of the best-fit parameters and the limits in the applicability of the model.

1-3. The Spectrum of ^{6}Li

The level scheme of the ^{6}Li nucleus is given in figure 1. According to the shell model the ^{6}Li nucleus consists of the complete 1s shell, containing two protons and two neutrons, plus one proton and one neutron in the 1p shell, i.e:, the ground configuration of ^{6}Li is $(1s)^4(1p)^2$.

With a purely central potential the ground configuration would be completely degenerate. Introduction of the interaction between the spin and orbital angular momenta of each particle and of two-body forces causes the degeneracy to be partially removed, the ground configuration splitting into levels corresponding to the different values of the total angular momentum J. The particles of the closed shell contribute zero angular momentum and positive parity, and may be ignored when computing the splitting of the ground configuration. Spin, parities, and relative energies of the lower levels of ^{6}Li are therefore those of a system of two particles, of quantum numbers $n_1=n_2=1$, $l_1=l_2=1$, $s_1=s_2=\tfrac{1}{2}$,

LEVEL DIAGRAM OF ^{6}Li
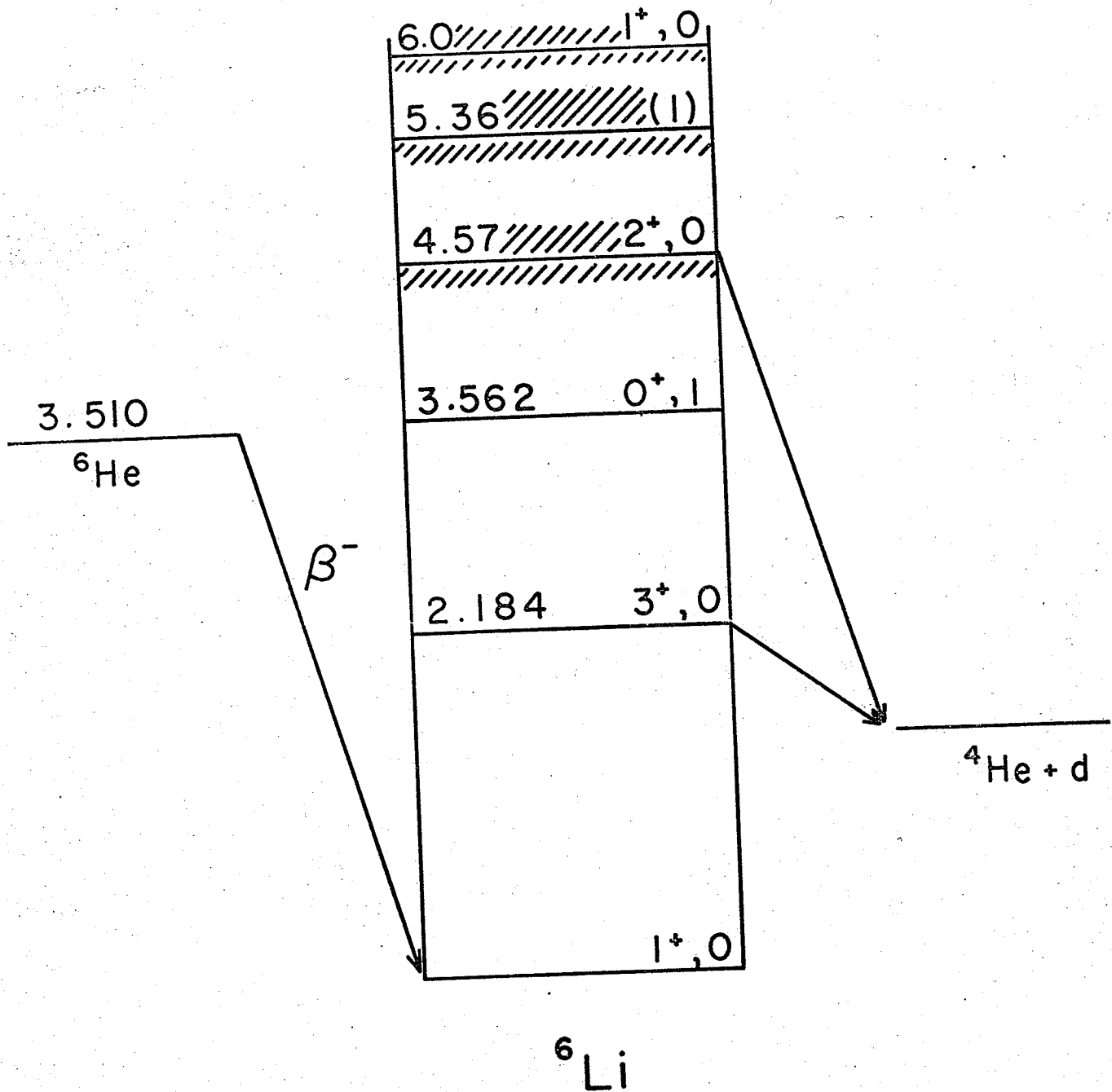
FIG. 1

$t_1 = t_2 = \frac{1}{2}$, $t_{z1} = \frac{1}{2}$, $t_{z2} = -\frac{1}{2}$, subject to the potential:

$$V_i = V_6 - a \, \underline{\ell}_i \cdot \underline{s}_i + V_{ij} \, .$$

The parity of all levels of the ground configuration is given by

$(-1)^{\ell_1 + \ell_2} = +1$; thus the states of negative parity whose existence

has been suggested between 6 and 14 MeV belong to some higher configu-

ration arising from the lifting of one p-nucleon to a higher shell.

The states of the ground configuration may be classified

according to the value of the total isospin T. States with T=1 have

the spin and space dependent part of the wave function antisymmetric

and are analagous to those obtained when the two particles in the 1p-

shell are both protons or both neutrons. The states with T=1 form

isospin triplets together with the corresponding states of ^{6}Be and ^{6}He

while the states with T=0 have the spin and space dependent part of the

wave function symmetric. The values of the total angular momentum are

obtained by coupling spins and orbital angular momenta of the two nuc-

leons. The level scheme obtained depends on the coupling scheme adopted.

If one supposes that in the potential the spin-orbit term is

much larger than the two-body interaction it is reasonable to use the

j-j-coupling:

$$\underline{\ell}_1 + \underline{s}_1 = \underline{j}_1 \quad , \quad \underline{\ell}_2 + \underline{s}_2 \; \underline{j}_2 \quad , \quad \underline{j}_1 + \underline{j}_1 = \underline{J} \quad (*)$$

(*) Here and in the following the symbols used are self explanatory and
conform to the usual practice.

$$\psi_{JM}^{j_1 j_2} = \sum (\ell_1 m_{\ell_1} \tfrac{1}{2} m_{s_1} | j_1 m_{j_1})(\ell_1 m_{\ell_2} \tfrac{1}{2} m_{s_2} | j_2 m_{j_2}) \,^{(*)}$$

$$\cdot (j_1 m_{j_1} j_2 m_{j_2} | JM) \, \phi_{\ell_1 m_{\ell_1}} \phi_{\ell_2 m_{\ell_2}} X_{\tfrac{1}{2} m_{s_1}} X_{\tfrac{1}{2} m_{s_2}}$$

Considering the two-body interaction as a perturbation, then in zero order approximation states with the same values of j_1 and j_2 but different J and M are degenerate, and the levels of the $(p)^2$ configuration are obtained by letting the two nucleons occupy independently single particle states. The single particle levels of the p-shell are $p_{3/2}$ and $p_{\frac{1}{2}}$, the former being the lowest, so that, neglecting the two-body interaction completely, the states of $(p)^2$ configuration are given by $(p_{\frac{3}{2}})^2$, $p_{3/2} p_{\frac{1}{2}}$, $(P_{\frac{1}{2}})^2$, in order of increasing energy. Introducing the perturbation due to the two-body interaction the multiplet $(p_{\frac{3}{2}})^2$ splits according to the different values of J. These are determined in the following way. We can write:

$$\psi_{JM}^{3/2 \ 3/2} = \sum_m (\tfrac{3}{2} M \tfrac{3}{2} M-m | JM) \psi_{3/2m}(1) \psi_{3/2M-m}(2)$$

$$= \pm \sum_m (\tfrac{3}{2} m \tfrac{3}{2} M-m | JM) \, \psi_{3/2m}(2) \, \psi_{3/2M-m}(1)$$

$$= \pm \sum_m (\tfrac{3}{2} M-m \tfrac{3}{2} m | JM) \, \psi_{3/2M-m}(2) \, \psi_{3/2m}(1)$$

where the sign on the right hand side is + for T=0 states, (which are symmetric with respect to the exchange of the space and spin coordinates

---

(*) $(j_1, m_1, j_2, m_2 | j_3, m_3)$ denotes the Chebsch-Gordon coefficient for the coupling of the angular momenta $\underline{j_1}$ and $\underline{j_2}$ to $\underline{j_3}$

of the two nucleons) and is - for T=1 states. Using the following

property of the Clebsch-Gordon coefficients:

$$(j_1 m_1 j_2 m_2 | JM) = (-1)^{j_1 + j_2 - J} (j_1 m_2 j_2 m_1 | JM)$$

we have:

$$\psi_{JM}^{3/2\ 3/2} = \pm(-1)^{3-J} \sum_m (\tfrac{3}{2}\ m\ \tfrac{3}{2}\ M-m | JM)\ \psi_{3/2 M-m}(2)\ \psi_{3/2 m}(1)$$

$$= \pm(-1)^{3-J}\ \psi_{JM}^{3/2\ 3/2}$$

Thus the values of J for the multiplet $(p_{3/2})^2$ are even if T=1 and odd

if T=0, and spin and isospin of the first four states are(J=3,T=0)

(J=1, T=0)(J=2, T=1),(J=0, T=1). This conclusion does not agree

with the experimental results, which suggest T=0 for the J=2(4.57MeV)

state.

The question of the applicability of the j-j model to the 1p

shell nuclei has been examined in detail by Kurath {8}. This author,

using the Hartree method and assuming j-j coupling, calculated the

matrix elements of a two-body interaction of the form $V_{12} = P\exp\{ -(\tfrac{r_{12}}{r_o})^2\}$

for the cases in which P is the Wigner, Majorana, Bartlett or Heisenberg

operator. A comparison with the results obtained fifteen years earlier

by Feenberg and Wigner {9} and Feenberg and Phillips {10} in L-S coup-

ling shows that, while both models predict correctly the spins in some

cases, none of them accounts satisfactorily for the spectra of all the

1p-nuclei. In particular, in the case of ^{6}Li, according to the j-j

coupling model the order in increasing energy of the lower states is

(3,0) (0,1) (1,0) (2,1), while experimentally the ground state is

(J=1, T=0), which is given correctly by the L-S model. The L-S coupling scheme is defined by:

$$\underline{\ell}_1 + \underline{\ell}_2 = \underline{L}$$

$$\underline{s}_1 + \underline{s}_2 = \underline{S} \quad \underline{L} + \underline{S} + \underline{J}$$

$$\psi_{JM}^{LS} = \sum (\ell_1 m_{\ell_1} \ell_2 m_{\ell_2} | LM_L)(\tfrac{1}{2}m_{s_1}\tfrac{1}{2}m_{s_2} | SM_S)$$

$$\cdot (LM_L SM_S | JM) \; \psi_{\ell_1 m_{\ell_1}} X_{\frac{1}{2}m_{s_1}} \psi_{\ell_2 m_{\ell_2}} X_{\frac{1}{2}m_{s_2}}$$

For two p-nucleons the possible values of the quantum numbers L,S,J are given by:

$$L=0,1,2 \quad ; \quad S=0,1 \quad ; \quad J= |L-S|, \ldots, L+S-1, \; L+S$$

The value of the total isospin is determined by symmetry considerations. The space dependent part of the wave function has symmetry given by

$\phi(1,2) = (-1)^L \; \phi(2,1)$ and the spin part is antisymmetric for singlet

states (S=0) and symmetric for triplet states (S=1). The spin-space

dependent wave function is then antisymmetric for even singlets and odd

triplets, which will correspond to T=1, while we shall have T=0 for odd

singlets and even triplets. Therefore the states of the $(p)^2$ configuration

in L-S coupling are given by the following table:

L	S	J	T	$^{2T+1,2S+1}L_J$
0	0	0	1	$^{31}S_0$
0	1	1	0	$^{13}S_1$

con't.

L	S	J	T	$^{2T+1,2S+1}L_J$
1	0	1	0	$^{11}P_1$
1	1	0	1	$^{33}P_0$
1	1	1	1	$^{33}P_1$
1	1	2	1	$^{33}P_2$
2	0	2	1	$^{31}D_2$
2	1	1	0	$^{13}D_1$
2	1	2	0	$^{13}D_2$
2	1	3	0	$^{13}D_3$

In the case of pure L-S coupling and of a central potential the
levels corresponding to the same values of L and S are degenerate. Feenberg
and Phillips {9} give the energies of the various multiplets in terms
of direct and exchange integrals of the Hartree theory:

$$\lambda = \int \psi(1)\phi(2)V_{12}\,\psi(1)\phi(2)d\tau_1 d\tau_2,$$

$$\kappa = \int \psi(1)\phi(2)V_{12}\phi(1)\psi(2)d\tau_1 d\tau_2,$$

where ψ and ϕ are two single particle wave functions. The indices 1
and 2 refer to the coordinates of the two nucleons and V_{12} is the inter-
action potential. The resulting order of the levels depends on the
exchange character of the interaction and on the wave functions.

The intermediate coupling theory of the lp-shell nuclei is
due to Inglis {11,12} and Kurath {13}. These authors describe the sys-
tem of the n nucleons of the $(1p)^n$ configuration by a Hamiltonian of
the form:

(9) $H = \sum_i T_i + \sum_{i>j} V_{ij}(r_{ij})O_{ij} + \sum_i a\underline{l}_i \cdot \underline{s}_i$,

where T_i is the kinetic energy operator for the ith nucleon, $\underline{l}_i$

and $\underline{s}_i$ are the orbital and spin angular momenta, $V_{ij}(r_{ij})$ is a cen-

tral two-body interaction and O_{ij} an exchange operator between nuc-

leons i and j. The radial dependence of V_{ij} is assumed to be

gaussian, the single particle wave functions are taken of the harmonic

oscillator type, and the exchange operator O_{ij} is chosen to be the

following linear combination of the space-exchange (Majorana) operator

P and of the spin-exchange (Bartlett) operator Q:

$$O_{ij} = 0.8\ P + 0.2\ Q.$$

Having specified the interaction, the ratio of the direct to the ex-

change integral λ/κ depends only on the strength of the nuclear force

and on the nuclear radius. Inglis and Kurath estimate $\frac{\lambda}{\kappa} = 6$ to be a

reasonable value for the 1p-shell. In the L-S coupling limit, which

is obtained by setting $a=0$ in eq.(9), the order of the levels is now

determined and their spacing depends only on κ, which is left as a

free parameter in order to compare more easily the prediction of the

theory to the experimental results. For the $(1p)^2$ configuration the

order of the ^{2S+1}L multiplets is ^3S, ^3D, ^1S, ^1D, ^3P, ^1P.

The transition to intermediate coupling is described in terms

of the parameter $\frac{a}{\kappa}$, which measures the relative strength of the spin-

orbit coupling and of the two-body interaction. When $a \ll \kappa$ the des-

cription of the system in terms of the L-S model is still valid, but the

coupling term $\sum_i a\underline{l}_i \cdot \underline{s}_i = A\ \underline{L} \cdot \underline{S}$, acting as a perturbation, removes the

degeneracy among levels of the same multiplet ^{2S+1}L. At the opposite

limit, when a>> K, the spin orbit term dominates the interaction, and the

(j-j) model is applicable. Numerical solutions, obtained by Inglis and

by Kurath for the various mass numbers corresponding to the lp-shell,

give position and spacing of the levels as a function of the parameter

$\frac{a}{K}$. The value of this parameter which best describes each nuclide is

then determined by comparison with the observed spectra.

In the case of ^{6}Li this value is given by $\frac{a}{K} \approx 1.3$, which is

much lower than the values obtained for heavier nuclei of the lp-shell

(≈ 5), and corresponds to essentially L-S coupling, the spin orbit int-

eration representing only a perturbation which causes the splitting of

the multiplets ^{2S+1}L.

In the preceeding we have discussed the spectrum of ^{6}Li from

the point of view of the shell model. Another possible approach is rep-

resented by a description in terms of an α-cluster deuteron-cluster

model {14}. A general review of the cluster model of nuclei is given

by Wildermuth and McClure {15}.

According to the cluster model the ^{6}Li wave functions are writ-

ten as:

$$\psi_{ijk} = A\phi_i(\alpha)\phi_j(d) \, X_k(\alpha\text{-}d)$$

where $\phi_i(d)$ is the internal wave function for the α-cluster, which de-

pends on the space, spin and isospin coordinates of the four nucleons,

$\phi_j(d)$ is the analagous wave function for the d-cluster, $X_k(\alpha\text{-}d)$ corres-

ponds to the relative motion of the two clusters and A is the antisymmetriz-

ation operator.

In the simplest formulation of the model (α), $\phi(d)$, and $X(\alpha-d)$ are taken to be harmonic oscillator wave functions with the same oscillator parameters. The ground state and the lowest excited state are assumed to correspond to a situation in which there is no internal excitation of the clusters. Since $S=0$, $T=0$ for the α-cluster and $S=1$, $T=0$ for the deuteron cluster, the wave functions obtained will correspond to $S=1$, $T=0$.

The orbital angular momentum for the relative motion is determined by the requirement that the lowest eigenvalue for the hamiltonian: [*]

$$E_{n\ell} = \{2(n-1) + \ell + \frac{3}{2}\}\, n\, \omega + \frac{3}{2}\, \hbar\omega + E_\alpha$$

be the same as obtained in the single particle model. Since we have two particles in the 1p shell, the lowest eigenvalue is $2(1+\frac{3}{2})\,\hbar\omega + E_\alpha$. We have then $2(n-1) + \ell = 2$ and the wave function for the relative motion corresponds to either 2s or 1d. The first case corresponds to the ground state:

$$\ell=0, \quad S=1, \quad J^\pi=1^+ ,$$

while the second corresponds to the lowest T=0 excited state:

$$\ell=2, \quad S=1, \quad J^\pi=3^+,\ 2^+,\ 1^+.$$

The lowest T=1 states are determined considering an unexcited α-cluster plus a deuteron cluster in the singlet state, $(S=0, T=1)$. Again, since the corresponding single particle configuration is $(1p)^2$ the possible values for ℓ are 0,2 and we obtain for the lowest two T=1 states.

------

[*]   The second term on the right hand side is the internal energy of the unexcited d-cluster. The internal energy of the α-cluster, E_α, is assumed to be the same as the energy of the α core in the shell model description.

$$\ell=0 \qquad S=0 \qquad J^{\pi} = 0^{+},$$

$$\text{and} \qquad \ell=2 \qquad S=0 \qquad J^{\pi} = 2^{+}.$$

It should be noted that, although the shell model description and the cluster description could appear quite different, when proper consideration is given to the identity of the particles the difference between the two points of view results to be merely a matter of perspective. From a physical point of view, the fact that there is a high probability of finding four nucleons near each other to form an α-cluster does not contradict a quasi-independent motion of the nucleons, since any four among all the nucleons can, at any given instant, belong to the cluster. From a mathematical point of view, for the simple case of harmonic oscillator wave functions with the same parameters, it can be shown that, after proper antisymmetrization, the α-d cluster wave function becomes identical to the wave function obtained, on the basis of the shell model, by coupling in the L-S scheme two harmonic oscillator wave functions.[*] However, when refined versions of the two models are considered, the wave functions obtained are no longer identical.

1.4 Objectives of the Present Experiment

The optical model is remarkably successful when applied to medium and heavy nuclei. For these nuclei it is possible to determine "overall" potentials, with geometrical parameters fixed and dynamical parameters equal to given functions of energy which give good fits over a wide range of energies. Overall potentials for proton scattering in the range of 10-20 MeV have been determined by Perey {16} and Rosen et al. {17}. The potential obtained by Perey is given by:

---

[*] An explicit calculation is given in the book of Wildermuth and McClure {15} for the analogous case of the α-α cluster model of ^{8}Be.

$$V = 53.3 \text{ MeV} - 0.55E + (27 \frac{N-Z}{A} + 0.4 \frac{Z}{A^{1/3}}) \text{ MeV}$$

$$W_D = 3A^{1/3} \text{ MeV} \quad ; \quad V_s = \begin{cases} 8.5 \text{ MeV if } E \geq 17 \text{ MeV} \\ 7.5 \text{ MeV if } E < 17 \text{ MeV} \end{cases}$$

$$r = r_D = r_s = 1.25 \text{ fm} \quad ; \quad a = a_s = 0.65 \text{ fm.}, \quad a_D = 0.47 \text{ fm.}$$

The analysis of Rosen et al. led to the potential:

$$V = 53.8 \text{ MeV} - 0.33 E$$

$$W_D = 7.5 \text{ MeV} \quad ; \quad V_s = 5.5 \text{ MeV}$$

$$r_o = r_D = r_s = 1.25 \text{ fm.} \quad ; \quad a = a_s = 0.65 \text{ fm} \quad ; \quad a_o = 0.7 \text{ fm.}$$

Analyses at higher energies show that some modification is necessary.
In the range of 30-40 MeV the energy dependence of the real central
well becomes:

$$V = 49.9 \text{ MeV} - 0.22E + (26.4 \frac{N-Z}{A} + 0.4 \frac{Z}{A^{1/3}}) \text{ MeV}$$

(Fricke et al. {18}). At energies >30 MeV the radius of the imaginary
potential becomes greater than that of the real part (Hodgson{19} ,
Johanson et al {20} , Fricke and Satchler {21} , Fricke et al. {18}).
At 40 MeV the optimum geometrical parameters are:

$$r_o = 1.16 \text{ fm.} \quad ; \quad a = 0.75 \text{ fm.} \quad ; \quad r_W = 1.37 \text{ fm.}$$

$$a_W = 0.63 \text{ fm.} \quad ; \quad r_s = 1.064 \text{ fm.} \quad ; \quad a_s = 0.738 \text{ fm.}$$

It should be noted that at these energies $r_s < r_o$.

The optical model is less successful for light nuclei ($A \leq 16$).
This can be expected on the basis of the following considerations. On
one hand the basic idea of the model, that the interaction of the incident
nucleons with the A nucleons of the nucleus can be represented by an aver-

age one-body potential, may be expected to be a better approximation when A is large than when only few nucleons are present. On the other hand, when A decreases the number of states available in a given energy range decreases, and the effect of isolated resonances in the compound system is felt also at relatively high energies.

Examples of optical model studies of light nuclei are the investigations of the systems p + ^{12}C and p + ^{16}O. In the case of C^{12} irregularities in the energy dependence of the differential cross-section and polarization angular distributions between 20 and 30 MeV have been explained by resonances in the compound system ^{13}N (Dickens et al. {22, 23}, Craig et al.{24}). An optical model study of the elastic scattering of protons by ^{12}C, at 30,40 and 50 MeV has been carried out by Fannon et al. {25}. The geometrical parameters which correspond to the best fits obtained by these authors are quite close to those for medium and heavy nuclei, but the quality of the fits is generally not as good. At 40 MeV Fannon et al. could obtain a good fit to polarization data at backward angles only by letting a_s decrease to very small values (~ 0.1 fm.). While at 30 and 50 MeV the calculations of these authors produce reaction cross-sections in agreement with values interpolated from total reaction cross-section measurements on neighboring nuclei, at 40 MeV it was not possible to obtain simultaneously good fits to polarization and differential cross-section data and an acceptable value for the reaction cross-section. An optical model analysis of elastic scattering of protons from ^{16}O has recently been published by van Oers and Cameron {26}. The data analysed were differential cross-sections and polarizations

in the energy range of 23 - 53 MeV. These authors were especially

interested in the energy dependence of the strength of the potentials,

therefore an optimum set of averaged geometrical parameters was deter-

mined and the analysis was carried on with fixed geometry. The optimum

geometrical parameters and the energy dependence of the real central

potential do not differ greatly from those obtained at comparable ener-

gies for medium and heavy nuclei. However, the quality of the fits ob-

tained for the differential cross-sections is only fair and the agreement

between the calculated and experimental polarization angular distribu-

tions is only qualitative. The quality of the fits deteriorates for ener-

gies $\lesssim 30$ MeV. This is consistent with the observed nonmonotonic energy

behaviour observed in this energy region, which has been attributed to

resonances in the compound system ^{17}F.

One of the objectives of the present experiment was to further

investigate the applicability of the optical model to light nuclei. ^{6}Li

appeared to be a highly suitable target for this purpose, since it is

probably the lightest nucleus for which macroscopic concepts and models

may be expected to apply. An investigation of the applicability of the

optical model to ^{6}Li can be considered as consisting of two parts. The

first part is a test of the possibility of obtaining fairly good fits with

reasonable values of the parameters. A negative result on this test

would put in question the possibility of representing the interaction of

the incident proton with the ^{6}Li nucleus by means of an average one-body

potential. This would imply a complete failure of the optical model. On

the other hand, should one be able to obtain reasonable fits, not all the

questions regarding the applicability of the optical model to ^{6}Li

would be settled, since the model can be considered completely success-

ful only if the fits are obtained with parameters which vary slowly and

regularly with energy and mass number. The second part of the investi-

gation consists therefore in fitting the data with the geometrical para-

meters kept fixed to optimum averaged values, and comparing these values

and the dynamical parameters obtained with those for other light nuclei.

When doing such comparisons one should, however, not overlook the follow-

ing point. It has been shown (Cole et al. {27}, Perey {28}) that, when the

elastic channel is strongly coupled to inelastic channels, the optical

potential obtained by fitting the elastic scattering alone may be quite

different from that obtained by fitting the elastic and inelastic data

together, and that it is the latter that may be expected to vary regular-

ly from nucleus to nucleus. In the case of ^{6}Li the differential cross-

section for scattering from the ($J^\pi = 3^+$, T = 0) 2.184 MeV level is,

except at the most forward angles, comparable to that for elastic scat-

tering. Neglecting the coupling may therefore affect the results in a

significant way.

In order to take into account the coupling between the elastic

and inelastic channels and obtain simultaneous fits of the elastic and

inelastic data, one has to resort to a generalization of the optical model

which is known as the coupled-channel approximation (Chase et al {29},

Buck {30}, Tamura {31}). This approach consists in expanding the complete

wave function in a series of eigenfunctions of the total angular momentum

of the system. For each entrance channel (specified by the spin of the

target nucleus and the total and orbital angular momenta of the inci-

dent proton) the angular momentum eigenfunctions are expressed as a

sum of products of elastic and inelastic scattering wave functions

and nuclear wave functions corresponding to the ground state and to

those excited states which one wants to take into account explicitly.

By inserting these angular momentum eigenfunctions in the Schrödinger

equation one obtains a set of coupled differential equations. The reac-

tion channels not considered explicitly are taken into account by in-

cluding an absorptive part in the interaction potential. In order to

solve the coupled equations one has to specify the interaction. In

the case of collective nuclei the interaction can be represented by a

potential having the same general form as the optical potential, but with

a non-spherical real central well. This potential can be easily expres-

sed, to first order, as the sum of the ordinary (spherical) optical po-

tential and a term proportional to the parameter describing the permanent

or dynamical deformation.

All the coupled-channel calculations done to date are relative

to the case of collective nuclei. The theory can be formulated in a quite

general way, and there exist a number of computer codes which may be used

in calculations for many collective nuclei. A direct use of these codes in

the case of ^{6}Li is not possible, since the ^{6}Li spectrum can not be des-

cribed by a collective model in a straight forward way. It is possible,

however, to rewrite the cluster model wave functions in a form which ex-

hibits a collective character[*] and one may hope along these lines to be

----

(*) see Wildermath and McClure {15}, chapter IV, section E.

able to formulate the coupled-channel calculation for ^{6}Li in a form

which differs from the usual collective model formulation only in

details. The feasibility of such a program is currently under study.

Another objective of the present experiment was the measure-

ment of angular distributions for the scattering from the ($J = 0^+$, $T = 1$)

3.562 MeV level and their analysis in terms of a microscopic theory.

In the microscopic description of an inelastic scattering reac-

tion (Madsen {32}, Satchler {33}) the interaction of the incident proton

with the target nucleus is described by an effective potential V_{eff} which

is assumed to be the sum of the two body interactions of the incident pro-

ton with the active nucleons of the target.

$$(10) \quad V_{eff} = \sum_k v_{kp}$$

Neglecting tensor forces and spin-orbit forces, a general form of the

two-body interaction v_{kp} is given by:-

$$(11) \quad v_{kp} = V_0(|\underline{r}-\underline{r}_k|) + V_\sigma (|\underline{r}-\underline{r}_k|)(\underline{\sigma}_k \cdot \underline{\sigma}_p) + V_\tau(|\underline{r}-\underline{r}_k|)(\underline{\tau}_k \cdot \underline{\tau}_p)$$

$$+ V_{\sigma\tau}(|\underline{r}-\underline{r}_k|) (\underline{\sigma}_k \cdot \underline{\sigma}_p) (\underline{\tau}_k \cdot \underline{\tau}_p)$$

where $\underline{r}$ and $\underline{r}_k$ are the position of the incident proton and of the kth

nucleon relative to the center of mass of the target, and $\underline{\sigma}_k, \underline{\sigma}_p, \underline{\tau}_k, \underline{\tau}_p$

are the spin and isospin operators.

In the framework of the distorted wave Born approximation the

transition amplitude for inelastic scattering is given by:

$$(12) \quad T_{fi} = \int X_f^{(-)*}(\underline{k}_f,\underline{r})(\psi_f|V_{eff}|\psi_i) \, X_i^+(\underline{k}_i,\underline{r})d^3r$$

where $X_f^{(-)}$ and $X_i^{(+)}$ are distorted waves, obtained from an optical potential which fits the elastic scattering data and depends on the relative position and momentum while ψ_f and ψ_i depend on the internal coordinates of the scattering system.

Assuming the same radial dependence for each term, the potential (10),(11) can be written in the form:

$$(13) \quad V_{eff} = V^{(0)} \cdot \underline{1} + V^{(1)} \cdot \underline{\tau}_p \,,$$

where

$$(14) \quad V^{(0)} = \sum_k V_{00} + V_{10}\underline{\sigma}_k \cdot \underline{\sigma}_p) \, g \, (|\underline{r}-\underline{r}_k|) \,,$$

$$(15) \quad V^{(1)} = \sum_k \underline{\tau}_k (V_{01}+V_{11}\underline{\sigma}_k \cdot \underline{\sigma}_p) \, g \, (|\underline{r}-\underline{r}_k|).$$

The right hand side of (13) is of the form $\sum_T V^{(T)} \cdot 0_T$, that is a sum of scalar products of tensors $V^{(T)}$, of rank T in the isospin space of the target, and tensors 0_T, of rank T in the isospin space of the projectile. Since the potential (13) is a scalar, the total isospin $\underline{T}_{target} + \underline{t}_p$ is conserved. Clearly the tensor $V^{(T)}$ may join states in which the nuclear isospin differs by T. Hence the isoscalar potential (14) cannot transfer isospin to the target, while the isovector potential (15) may transfer one unit of isospin.

Similarly, the right hand sides of (14) and (15) may be written as sums of tensors in the spin spaces of the target and of the incident proton. It may so be shown that the indices that identify the strengths V_{TS} of the various terms of the potential correspond to the isospin and

spin that may be transferred to the target nucleus.

The transition between the ground state of ^{6}Li ($J^\pi = 1^+$, T=0) and the second excited state ($J^\pi = 0^+$, T=1) correspond to T=1, S=1. In this case therefore the effective interaction reduces to

$$V_{eff} = \sum_k V_{11} (\underline{\sigma}_k \cdot \underline{\sigma}_p)(\underline{\tau}_k \cdot \underline{\tau}_p)\ g\ (|\underline{r} - \underline{r}_k|)$$

With the proper choice of the optical model parameters, the nuclear wave functions and the function $g(|\underline{r} - \underline{r}_k|)$, the differential cross-section can be calculated in terms of V_{11}, which may then be determined by comparison with experimental results.

Austin and Crawley {34} have measured and analysed the differential cross-section for the inelastic scattering from the second excited state of ^{6}Li at 24.5 MeV incident energy. In the analysis the states of ^{6}Li were described by L-S coupled harmonic oscillator wave functions, with an oscillator parameter of 1.9 fm. The interaction was chosen of Yukawa shape, with a range of 1.0 fm. A good fit to the experimental data for angles <50° was obtained with V_{11}=12.7 fm. The energy dependence of V_{11} has been studied by Austin et al.{35} from data for the total cross-section of the reactions ^{6}Li(p_1p_1)^{6}Li (3.562 MeV) and by Clough et al {36} from data for the angular distribution of the reaction ^{6}Li(p,n) ^{6}Be at 30 and 50 MeV. The results indicate that the strength of the spin-isospins dependent interaction is approximately constant over the range 20 to 50 MeV.

CHAPTER 2

2-1 Experimental Arrangement

The experiment was performed using the proton beam produced by the University of Manitoba sector-focused cyclotron {37}. The proton beam is obtained by accelerating negative hydrogen ions. Extraction from the cyclotron is accomplished by passing the ions through a 25μ thick aluminum foil, which strips off two electrons from each ion. Figure 2 shows the layout for the vault area and for the 45° right beam line used in the present experiment. The beam is deflected down the beam line by a combination magnet C. The quadrupole doublet $Q_1 - Q_2$ produces a horizontal waist in the beam cross-section. The steering magnets S_1 and S_2 are used to center the beam vertically along the beam line. A set of horizontal and vertical slits (slits 1) is located at the position of the waist. The beam is then momentum analysed by a 45° deflection through a bending magnet. A second set of slits (slits 2) transmits a suitable component of the beam into the experimental room, where the quadrupole doublet $Q_5 - Q_6$ produces a second waist at the center of the scattering chamber. Typical size of the beam spot at the target is 3mm. by 5mm. The scattering chamber is shown in figure 3. Detector cubes are positioned on two turn tables which can be rotated independently. The top table can hold only one detector cube while the bottom one can hold four cubes each separated by 10.0°. Accurately positioned holes on the tables and corresponding dowels in the cubes are used for positioning the detector cubes on the tables. The target mount can hold three solid targets and is lowered
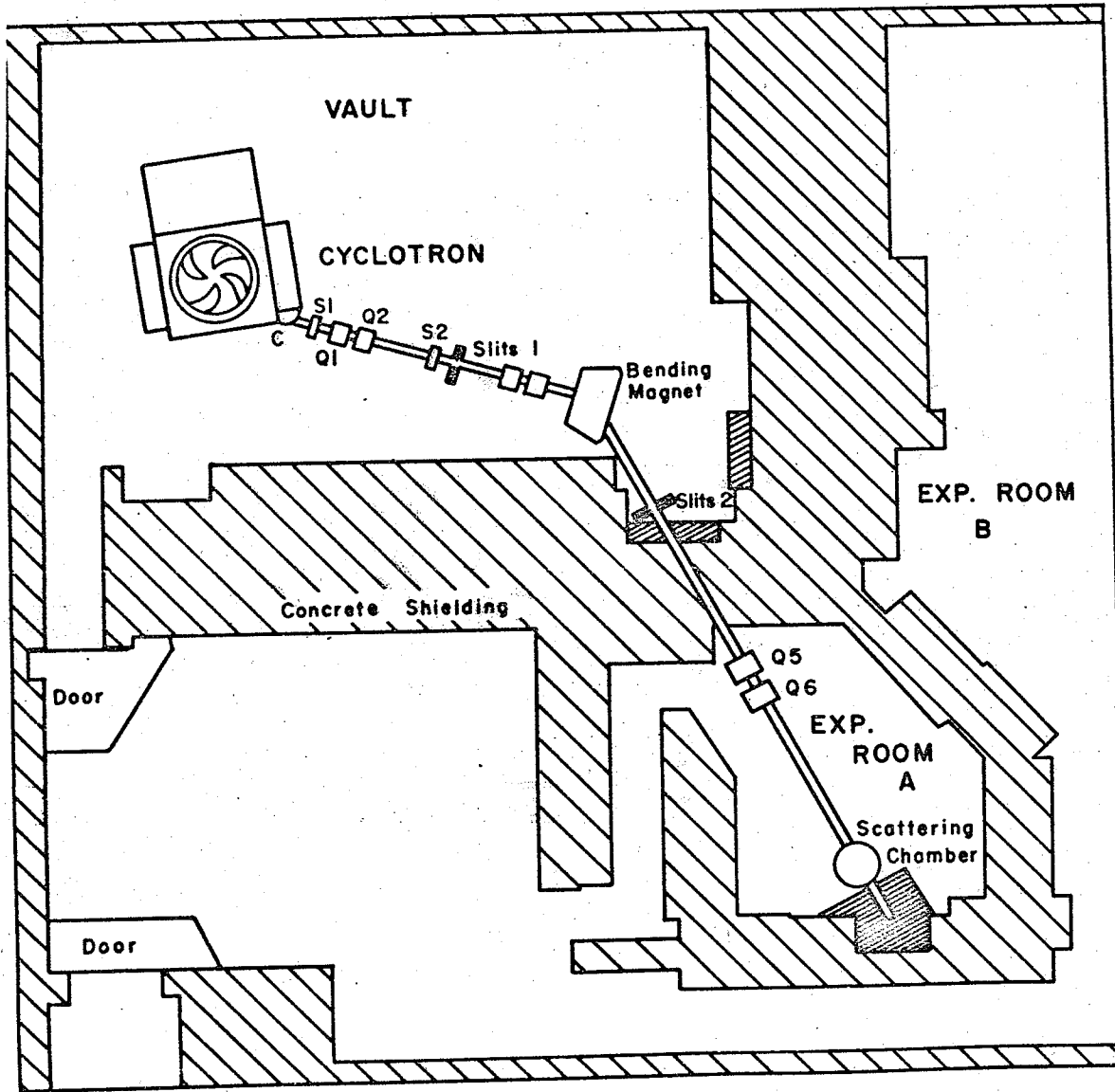
Fig. 2   Cyclotron Beam Line Layout.

a. TARGET HOLDER
b. DETECTOR CUBE
c. NaI MONITOR COUNTER
d CENTRAL POSITIONING
        CYLINDER
e. COOLING LINES
f. UPPER TABLE
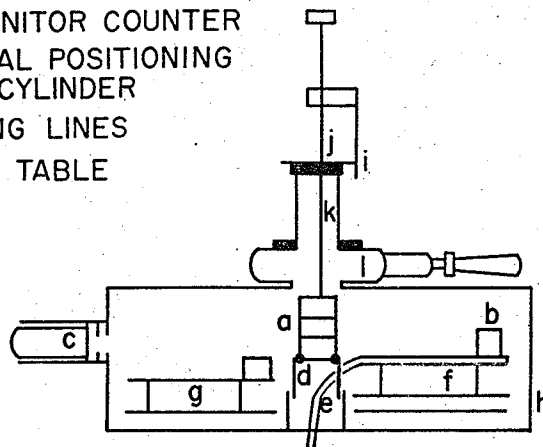
g LOWER TABLE
h. TABLE POSITION READOUT
i TARGET ANGLE READOUT
j TARGET MOUNT
k. TARGET MOUNT VACUUM LOCK
l. VACUUM VALVE

SCALE (inches)

Fig. 3   SCATTERING CHAMBER

from a vacuum lock mounted at the top of the chamber. Selection of

the target to be used, as well as the setting of the target angle, is

accomplished by the proper vertical and rotational positioning of the

target rod.

During the course of the experiment, a ZnS screen, mounted on

the target ladder, was used to check if the beam was correctly center-

ed and had the proper dimensions. The intensity of the incident beam

was measured by collecting the beam current in a Faraday cup, surround-

ed by steel bricks to reduce background radiation. The Faraday cup was

connected to a charge integrator (Brookhaven Instrument Corp. model

1000), whose digital output was fed to a scaler. The energy calibra-

tion of the proton beam was obtained by using the crossover method

with CD_2 and CH_2 targets {38} . The calibration measurements related

the beam energy to the bending magnet field strength, which was deter-

mined using an NMR system. The energy of the beam was known with an

accuracy of ± 0.2 MeV.

A ΔE-E detector telescope was mounted in a cube on the lower

turn table of the scattering chamber. A collimator, mounted in the

cube in front of the detector telescope, defined the solid angle of

acceptance. The diameters of the collimators used and their distances

from the center of the scattering chamber have been accurately measured.

Two NaI counters, set at 37.5° on the two sides of the scattering

chamber, were used to monitor any variation in the direction of the

beam. The targets were made from isotopically enriched (99.3%) ^{6}Li

metal. The characteristics of the nine self-supporting targets used

in the course of the experiment are given in the following table:

Target	Measured Thickness	Method of Preparation
#1	13.89 mg/cm^2	pressed powder
#2	6.61 mg/cm^2	"
#3	9.05 mg/cm^2	"
#4	4.62 mg/cm^2	"
#5	6.26 mg/cm^2	"
#6	4.84 mg/cm^2	"
#7	2.67 mg/cm^2	evaporation under vacuum
#8	3.45 mg/cm^2	"
#9	2.30 mg/cm^2	"

The thickness of the thicker targets was determined by weighting a portion of known area taken from the center of the target. The thickness of targets 7 to 9 was determined using known range energy relations from the energy loss of α-particles (from both ^{241}Am and ThC sources) which have traversed the target. The ΔE silicon surface barrier detectors and E Lithium drifted silicon detectors had the following thicknesses:

Energy	ΔE (Surface Barrier)	E(Li-Drifted Silicon)
25.9 MeV	200μ	5mm.
29.9 MeV	200μ	3mm. + 5mm.
35.0 MeV	200μ	3mm. + 5mm.
40.1 MeV	200μ	5mm. + 5mm.
45.4 MeV	200μ	5mm. + 5mm.

Diagram of the Electronics

Fig. 4

33.

A block diagram of the electronics is given in figure 4. All components indicated were manufactured by Canberra Industries, with the exception of the particle identifier (ORTEC, Model 423). This unit operates according to the Goulding-Landis identification method {38}. The energies lost in the E and ΔE detectors are related by:

$$\frac{T}{a} = (E + \Delta E)^{1.73} - E^{1.73}$$

where T is the thickness of the ΔE detector and a is a constant which depends on the type of the incident particle but is approximately independent of its energy. This formula is derived from the empirical range-energy relationship $R = aE^{1.73}$, and gives a quantity which is characteristic of each type of particle. When the pulse from the E detector, the pulse from the ΔE detector and the enable pulse arrive in coincidence at the particle identifier, the unit produces two output pulses: an E + ΔE pulse, proportional to the total energy of the particle, and a particle identifier output (P.I.O.) pulse, whose height depends on the type of incident particle. The E + ΔE pulse was fed to a Nuclear Data 160 dual analog to digital converter (ADC). The P.I.O. pulse was sent to a single channel analyser (SCA) and then to the ADC gate. The SCA window was set in such a way that only pulses corresponding to protons could open the gate. The ADC was interfaced to a PDP-9 computer, where the spectra were stored and recorded on DEC tape. A correction factor for the dead time of the ADC was obtained from the ratio of the counts recorded by the SCA scaler and the total number of counts recorded by the computer. A typical example of the spectra

^{6}Li + p   Proton Spectrum

E_p = 25.9 MeV

θ_{lab} = 19.8°

G.S.

× 1/32 →

2.18

3.56

COUNTS

CHANNEL   NUMBER
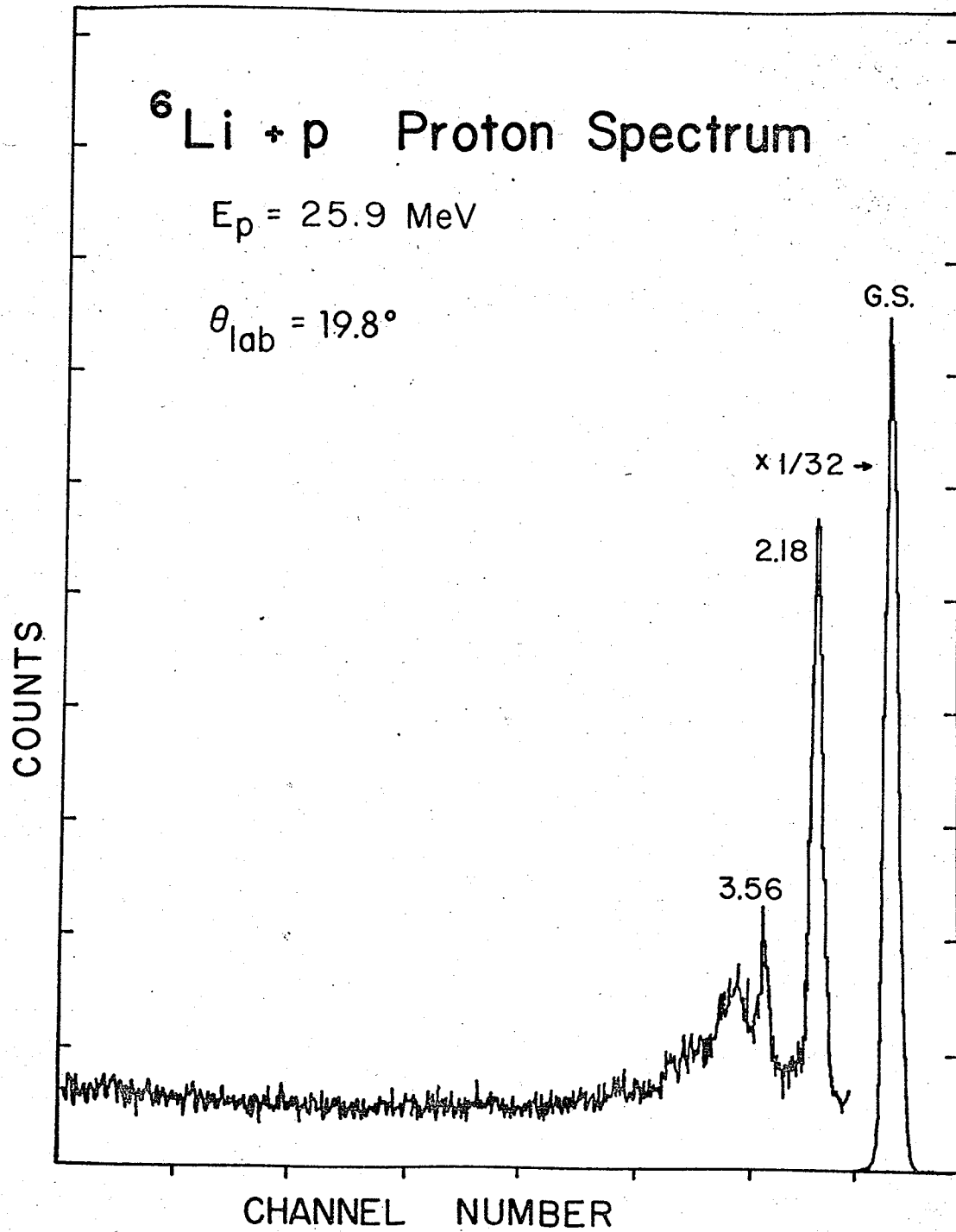
Fig. 5

obtained is shown in figure 5.

2-2. Data Reduction and Errors (Elastic Scattering)

The differential cross-section for the scattering of protons

from a pure isotope of mass number A is given by (*)

$$(16) \quad \frac{d\sigma}{d\Omega} = \left[2.660 \times 10^{-4} \times \frac{AY\tau\cos\phi}{Q\ t\ \Delta\Omega} \right] mb/sr. \quad ,$$

where Y is the number of counts in the peak, ϕ is the target angle,

which is defined as the angle between the normal to the target and

the incident beam director, τ is the dead-time correction factor,

Q is the charge collected (in nC), t is the target thickness in mg/cm^2

and $\Delta\Omega$ is the solid angle. If the target contains an admixture of a

second isotope of mass number A' and is contaminated by impurities of

mass numbers A_i, A_{i+1}...., the following corrections must be consider-

ed:

(i) In the numerator of (16) the atomic number A must be sub-

stituted with the quantity:

$$(17) \quad \mathcal{A} = A + \frac{1-\alpha}{\alpha} A'$$

where α is the ratio of the number of atoms of the species A to the

total number of atoms of the two species

$$\alpha = \frac{n_A}{n_A + n_{A'}}$$

(ii) In the denominator of (16) the measured target thickness

t must be substituted with an effective target thickness.

(*) Formulas (16), (17) and (18) are derived in appendix I

(18) $t_{eff} = t - t_i - t_{i+1} \cdots\cdots\cdots,$

where the "impurities target thickness" t_i, $t_{i+1}\cdots$ can be calculated

from the known values of the cross-sections for scattering of protons

by the contaminating nuclei (see appendix I).

(iii) At those angles where a proton peak due to elastic or in-

elastic scattering by a nuclide A_j (one of the impurities) overlaps

with the peak corresponding to the scattering by the isotope A, the

contribution due to the former must be subtracted from Y. This con-

tribution can be calculated from (16) in terms of the differential

cross-section for scattering by A_j:

$$Y_j = \frac{1}{2.661\text{x}10^{-4}} \frac{Q \, t_j \, \Delta\Omega}{A_j \, \tau\cos\phi} \left(\frac{d\sigma}{d\Omega}\right)_j$$

Setting $Y_o = Y - Y_j$ and substituting (16) one obtains the following

expression for the corrected differential cross-section $\left(\frac{d\sigma}{d\Omega}\right)_o$

(19) $\left(\frac{d\sigma}{d\Omega}\right)_o = \frac{d\sigma}{d\Omega} - \frac{A \, t_j}{A_j t} \left(\frac{d\sigma}{d\Omega}\right)_j$

A correction of this kind should also be applied to those spectra

where the elastic peak overlaps with peaks due to elastic and inelastic

scattering by the other isotope. If, however, the percentage of the

second isotope in the target is small, the corresponding inelastic

peaks may generally be neglected, and the correction given by (19) for

elastic scattering by the contaminating isotope approximately cancels

out with the correction (ii).

In practice the reduction of the data was performed according

to the following procedure. First the number of counts in the elastic

peak was determined using an appropriate program run off-line on the

PDP-9. Generally the spectra did not show any appreciable background

in the region corresponding to the elastic peak. An exception was re-

presented by the small angle spectra for 45.4 MeV incident protons

in which case proper subtraction was made. As a first step in the

data reduction the uncorrected differential cross-sections were comput-

ed by means of formula (16). Next the target thicknesses of the impur-

ities were determined for each of the targets used. This was done by

choosing for each target a spectrum in which the peaks due to elastic

scattering from the contaminating nuclei were clearly resolved. These

peaks were then integrated and the thicknesses were calculated from the

known values of the differential cross-sections for the contaminants.

The uncorrected differential cross-sections were multiplied by the

correction factor t/t_{eff}. The correction factor $\mathcal{A}/A$ was also applied

in all cases where the elastic peaks due to ^6Li and to ^7Li were resol-

ved. Finally, the results of kinematics calculations and energy cali-

bration were used to determine the position of the elastic and inelas-

tic peaks due to scattering by the impurities, and, whenever appli-

cable, the correction (19) was made. In several cases two or more

measurements of the differential cross-section were available for the

same scattering angle and incident energy. In particular, during the

measurement of the angular distribution at a given energy it was prac-

tice to repeat the measurement for those scattering angles at which

the target angle setting was changed. A weighted average of the diff-

erent measurements was taken, according to the formula:

$$\langle x \rangle = \frac{\sum\limits_{i=1}^{n} x_i/(\Delta x_i)^2}{\sum\limits_{i=1}^{n} 1/(\Delta x_i)^2}$$

where x_i (i=1,..n) are the different measurements and Δx_i the corresponding statistical error. The error of the weighted mean was calculated using

$$\Delta x = \frac{\sum\limits_{i=1}^{n} (x_i - \langle x \rangle)^2/(\Delta x_i)^2}{(n-1)\sum\limits_{i=1}^{n} 1/(\Delta x_i)^2}$$

In general the error was of the same order of magnitude as the statistical errors. This indicated the consistency of the different measurements.

The laboratory scattering angles could be measured with an accuracy of $\pm 0.1^\circ$. In order to detect any systematic error in the angle measurement, the cross-sections at forward angles were measured both left and right of the incident beam. The observed asymmetry was negligible in all but two cases, where a correction of 0.2° to the measured laboratory scattering angles had to be introduced.

The relative errors in the differential cross-sections were determined by taking into account:

    (i)   The statistical error

    (ii) The error due to the uncertainty in the scattering angle
           θ

    (iii) The error due to the uncertainty in the incident energy
           E_p

    (iv) The error in the dead time correction.

The total relative error $\Delta\sigma/\sigma$ (*) was obtained from the errors corresponding to the different contributions $\Delta\sigma_i$ as

$$\frac{\Delta\sigma}{\sigma} = \sqrt{\sum_i (\frac{\Delta\sigma_i}{\sigma})^2}$$

The errors (ii) and (iii) were obtained from:

$$\Delta\sigma_2 = \frac{\partial\sigma(\theta,Ep)}{\partial\theta} \Delta\theta \quad \text{and} \quad \Delta\sigma_3 = \frac{\partial\sigma(\theta,E_p)}{\partial Ep} \Delta E_p$$

with $\Delta\theta = 0.1^\circ$ and $\Delta E_p = \pm 0.2$ MeV. The error in the dead time correction was taken equal to 1/10 of the correction made. For $\theta \leq 130^\circ$ the error due to the uncertainty in the energy gave the greatest contribution, while at extreme backward angles the statistical error was generally the most important.

The order of magnitude of the different contributions to the relative error is given in the following table:

Error	Typical values
(i)	0.1-0.2% (small angles), 2-3% (large angles)
(ii)	0.5%(20°), 1%(60°), 0.1%(170°)
(iii)	1%(small angles), 3-4%(100°), 1.5% (large angles)
(iv) at 25.9 MeV	2%(small angles), 0.3%(angles $>90^\circ$)
at other energies	0.2-0.5%(small angles), <0.1% (angles $>90^\circ$)

___

(*) Here and in the following we write $\frac{d\sigma}{d\Omega} = \sigma$

In particular cases the following additional contributions to the

relative error were considered:

(v)   The error in the correction made when the elastic

peak overlaps with a peak due to scattering from

the impurities in the target (eg. (19))

(vi) The error in the background subtraction.

The error (v) was taken equal to 1/3 of the correction made.   The

error in the background subtraction was of the order of 1%.

The uncertainty in the normalization of the differential cross-

section was compounded from

(a)   The uncertainty in the determination of the solid angle

(b)   The uncertainty in the integration of the beam current

(c)   The uncertainty in the target thickness

(d)   The uncertainty in the determination of the incident energy.

The most important contribution to the total error in the normalization

was the uncertainty in the target thickness, which resulted not only

from errors in the measuring process, but also from the non-uniformity

of the target and from the error in the correction for contaminations.

The total error in the normalization was estimated to be of the order

of 10%.

2-3   Data Reduction and Errors (inelastic scattering)

The differential cross-section for inelastic scattering can be calculated from the formula:

$$(20) \qquad \frac{d\sigma}{d\Omega}\Big)_{in} = \frac{Y_{in}}{Y_{el}} \frac{d\sigma}{d\Omega}\Big)_{el}$$

where Y_{in} is the number of counts in the peak which corresponds to scattering from the level considered, Y_{el} is the number of counts in the elastic peak of the same spectrum and $d\sigma/d\Omega)_{el}$ is the elastic differential cross-section for the same energy and scattering angle.

The main problem in the reduction of the inelastic data was the extraction of peaks from the continuum resulting from three-body break-up reactions.   In the case of the (2.184 MeV) first excited state the background subtraction did not present serious difficulties since only the low energy side of the inelastic peak is appreciably affected by the background (see figure 5).   Two methods for the background subtraction were used.   In the first method, the PDP-9 and a CALCOMP plotter were used to obtain an enlarged graph of the peak and the background subtraction was done graphically.   The graphical method was applied twice to a whole series of spectra, and the results were found to be consistent within 1%.   The second method consisted of using a computer program to fit the experimental peak to a gaussian with a fixed horizontal baseline.   It was found that changing within reasonable limits the input parameters of the fit (peak position, width and baseline) the resulting values of the integrated peak varied by less than 1%.   It was also found that by applying the two methods to the same spectrum one obtained results in agreement within 1%.

Having determined the number of counts in the inelastic peaks,
the differential cross-sections were calculated from equation (20).
In the great majority of cases the values used for the elastic cross-
section had been previously derived from the same spectrum. Thus,
applying formula (20) was exactly equivalent to calculating the inelas-
tic cross-section by substituting Y_{in} for Y in the general formula
(16) and making the appropriate corrections. The errors could there-
fore be calculated in the same way as for the elastic scattering
differential cross-section, assuming an error of 1% in the background
subtraction. In the cases corresponding to $\theta_{lab} \leq 60°$, Ep=45.4 MeV,
however, the elastic cross-sections used had been extracted from diff-
erent data than those used to determine Y_{in} and Y_{el}(*). In these
cases, therefore, the quantities on the right hand side of (20) were
obtained from three independent measurements and gave independent con-
tributions to the total error.

In the case of the 3.562 MeV level the extraction of the peak from
the background was quite a difficult problem. This is already apparent
from the spectrum of figure 5, and the situation is even worse at
larger angles, where the peak becomes barely visible. The problem was
solved in the following way. The PDP-9 and the CALCOMP plotter were
used to plot the part of interest of the spectrum. The energies corres-
ponding to the three-body break-up threshold, to the elastic peak and

(*) The reason was the following. In the original data, used to
calculate $d\sigma/d\Omega)_{el}$, the resolution was not good enough to extract the
inelastic peaks. The experiment was therefore repeated. The second
time however, the counting rate was high, resulting in a large dead-time.

to the peaks of the first and second excited states were determined
from relativistic kinematics calculations. The spectrum was cali-
brated using the positions of the peaks corresponding to the ground
state and to the first excited state. Then a smooth curve was drawn
on the graph, starting from the threshold for the three-body break-up
and passing through the valleys on both sides of the peak. For each
one of the channels of interest, the number of counts above the curve
was determined from the graph, and the numbers so obtained were used
as input in a gaussian fitting routine. This code was the same as
used in the reduction of the data for the first excited state; however,
the baseline level was not kept fixed during the fitting procedure.

Care was taken in determining in each case the positions of the
peaks corresponding to excited states of carbon and oxygen. These
peaks were present in the spectrum because of impurities in the target.
When one such peak overlapped exactly with the peak corresponding to
the second excited state, the proper correction could be made by use
of formula (19). When, however, the overlap was partial, it was not
possible to obtain a correct background subtraction.

In three cases the entire background subtraction procedure was
applied twice, obtaining results which differed by 15 - 20%. A typical
error of 20% was therefore assumed for the differential cross-sections
for scattering from the 3.562 MeV level.

CHAPTER 3

3-1. <u>Results and Discussion (elastic scattering).</u>

The experimental result, for the elastic scattering differential cross-sections are given in the first five tables of appendix II and in Fig. 6, where the size of the points corresponds to the typical relative errors. The angular distributions show a uniform variation with incident proton energy. The diffraction like structure becomes more pronounced as the energy of the protons increases, with minima in the angular distributions shifting to smaller angles.

The potential used in the optical model analysis is of the standard form (eg. (7), chapter 1.), with pure surface absorption and a real spin-orbit term. The data included in the analysis are the differential cross-sections measured in the present experiment and the polarizations obtained by Hwang et al. {40} at 38.7 MeV and by Mani et al. {41} at 49.5 MeV. The analysis was performed using the automatic search code SEEK {42} in a modified version which allows one to vary the spin-orbit geometrical parameters independently and which uses a surface absorbtive potential of the derivative Woods-Saxon form.

In the search for the best fit parameters the following procedure was adopted. At first the geometrical spin-orbit parameters were kept fixed at r_s = 0.98 fm. and a_s = 0.20 fm.[*] The analysis was carried out searching for values of the remaining parameters which gave the best fits to the differential cross-sections and, at the same time, reasonable fits to the polarizations and reasonable values of the total reaction

---

[*] These values were taken from Ref. {36} and are the result of an unpublished analysis of the 49.5 data by Mani.
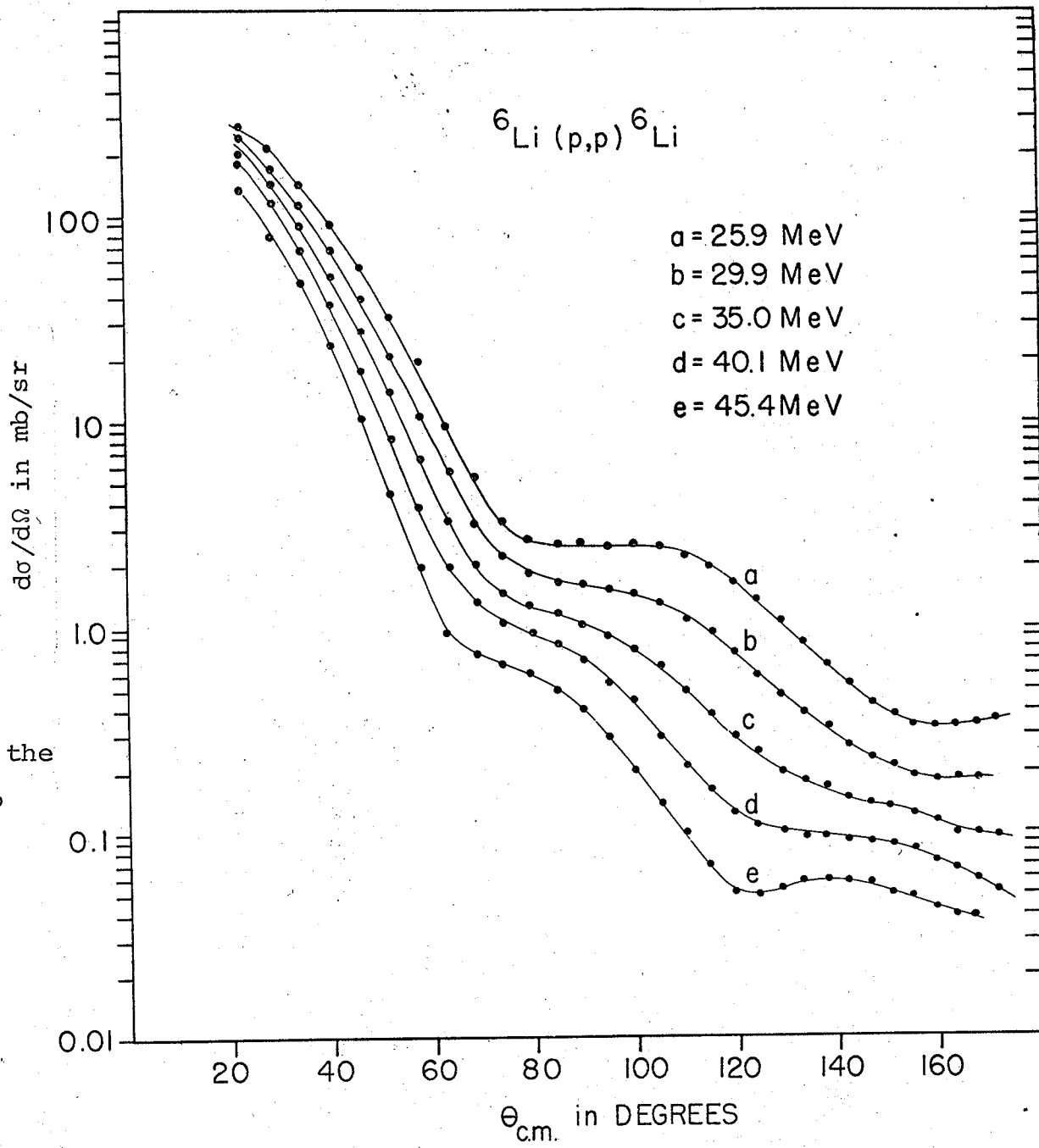
The curves are drawn to guide the eye and have no significance

^{6}Li (p,p) ^{6}Li

a = 25.9 MeV
b = 29.9 MeV
c = 35.0 MeV
d = 40.1 MeV
e = 45.4 MeV

Fig. 6

cross-sections. Since no experimental data were available for the

total reaction cross-sections, the theoretical results obtained were

compared with values extrapolated from data for nearby nuclei. Next,

the spin-orbit parameters were varied so as to optimize the fits to the

polarization data. Finally, r_s and a_s were fixed to the optimum values

obtained and the search on the remaining parameters was repeated. It

is well known that an indeterminacy exists for the parameters of the real

central part of the optical potential, so that equivalent fits can be

obtained with different values of the radius, provided that the depth of

the well is adjusted according to the rule Vr_0^n = const., with $n \approx 2$. In

order to facilitate the comparison of the potentials at the various

energies, the search was carried out with the radius parameter of the

real central term fixed to a suitable common value.

The program SEEK requires the polarizations to be fitted simul-

taneously to the differential cross-sections. A differential cross-

section angular distribution at 49.5 MeV has been obtained by Mani et al.

{41}. These data, however, were available only in graphical form and

there was a discrepancy between the normalization for these data and the

results of the present experiment.[*]   Since other measurements of the

differential cross-sections around 50 MeV were not available, the results

of   Mani et al. were extracted from the graph and renormalized. A

relative error of 10% was arbitrarily assigned to these data.

---

[*]   The normalization for the data of the present experiment at 40.1
      MeV agrees within 10% with the results of Chen and Hintz at
      39.7 MeV {43}.
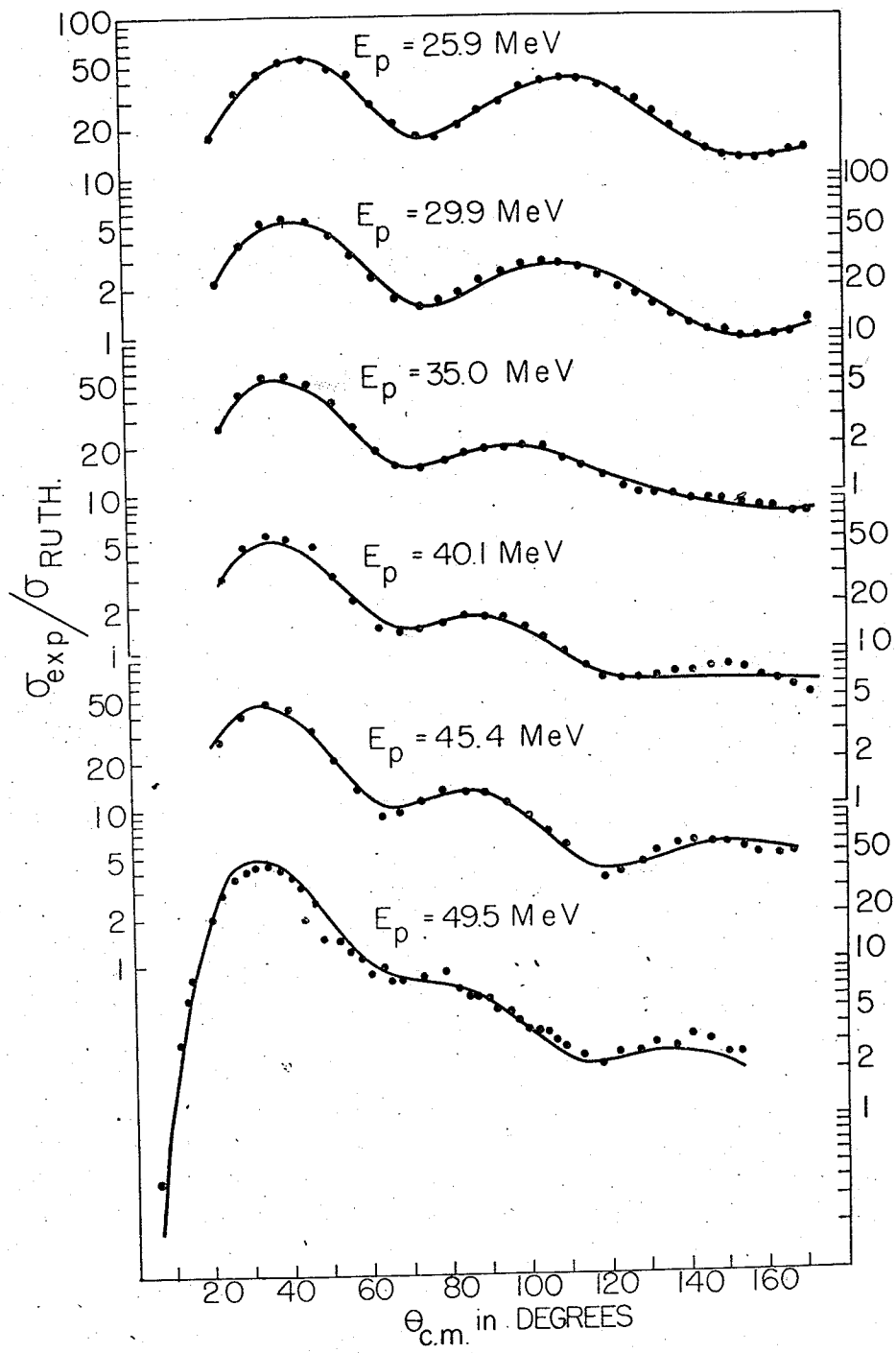
Fig. 7
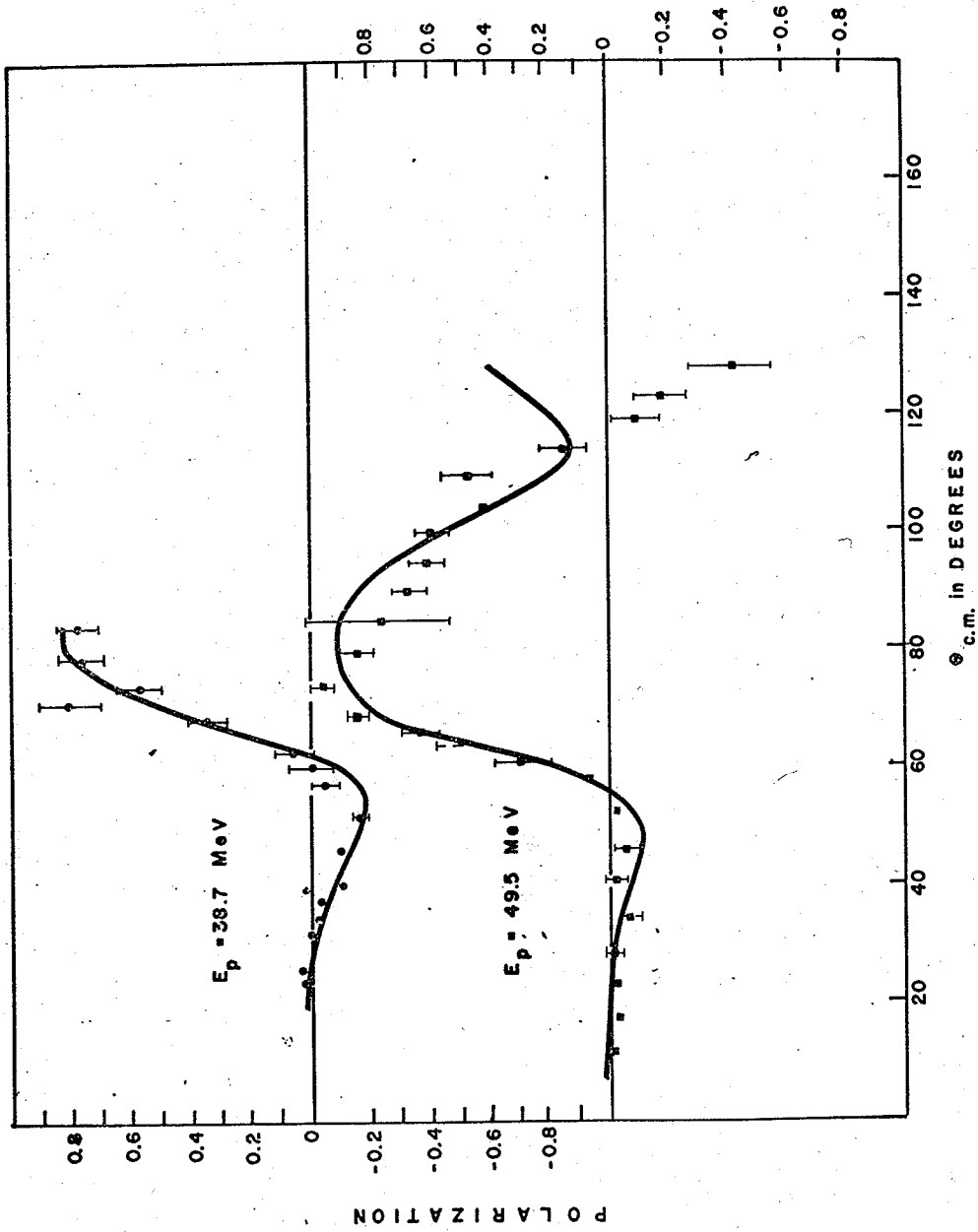
Fig. 8

A test done in the course of the analysis showed that, even at the higher energies, the inclusion of a small volume absorption term does not improve the fits appreciably.

The best fits obtained for the differential cross-section angular distributions are shown in Fig. 7, where the ratio of the differential scattering cross-section to the Rutheford cross-section is plotted versus the center of mass scattering angle. The results of the analysis of the 49.5 MeV data by Mani et al. are also included, even though one can not expect a very good fit in this case. Because of the large relative error assigned to these data, the differential cross-sections had less weight than the polarizations in the fitting of the 49.5 MeV data.

The best fits for the polarization angular distributions are shown in Fig. 8.

In the energy range 25-45 MeV. the fits obtained for the differential cross-sections are surprisingly good. At 49.5 MeV the general shape of the experimental angular distribution is well reproduced by the optical model calculation, but, not surprisingly, the height of the forward peak is slightly different in the theoretical and experimental curves. The fit to the polarization angular distribution at 49.5 MeV is quite good for angles up to 115° c.m. However, the negative values of the polarization experimentally observed at the larger angles are not reproduced. At 38.7 MeV a good fit has been obtained for the polarizations over the range 23° to 85° c.m. covered by the experimental data.

The optical model parameters which correspond to the best fits
are given in table 1. The quantities given are the dynamical and geo-
metrical parameters, the theoretical total reaction cross-section σ_{re}^{th} ,
the ratio χ_σ^2/N_σ of the χ^2 to the number of data points for the differen-
tial cross-sections, the corresponding quantity for the polarizations
χ_p^2/N_p , the typical relative error of the experimental differential
cross-sections $\Delta\sigma$ and the typical absolute error of the experimental
polarizations Δp. The total reaction cross-sections obtained by extrapo-
lation from experimental data for nearby nuclei are in the range 30-45
fm^2 at 25 and 30 MeV, 25-40 fm^2 at 35 MeV and 25-35 fm^2 at 40 and 45 MeV.
The values of σ_{re}^{th} obtained at the first five energies are therefore quite
reasonable. At 49.5 MeV an extrapolated experimental value of the total
reaction cross-section was not available, but σ_{re}^{th} seems to be quite
low as compared to the value at 45.4 MeV. The parameters obtained are
in general quite acceptable. The value 0.2 fm for the spin-orbit diffuse-
ness is rather small, but this is consistent with what has been found for
other light nuclei.

The most notable feature of the results obtained is the irregular
variation with energy of the diffuseness of the real central potential,
of the strength and the radius parameter of the imaginary potential and
of the strength of the spin-orbit potential. The energy dependence, how-
ever, is not erratic and the six sets of parameters can be quite naturally
divided into two groups, one corresponding to the energies of 25.9 and
29.9 MeV, the other corresponding to the energies greater than 30 MeV.
Within each group the strength of the real central potential decreases

TABLE 1 - BEST-FIT OPTICAL MODEL PARAMETERS

E_p (MeV)	V (MeV)	W_D (MeV)	V_s (MeV)	r_o (fm)	r_D (fm)	r_s (fm)	a (fm)	a_D (fm)	a_s (fm)	σ_{re}^{th} (fm^2)	χ^2_σ/N_σ	$\Delta\sigma$	$\dfrac{\chi^2_p}{N_p}$	Δp
25.9	59.15	10.14	12.15	(1.050)	1.334	(1.020)	0.288	0.568	(0.200)	43.4	0.667	3.5%	---	---
29.9	54.48	10.95	11.72	(1.050)	1.143	(1.020)	0.273	0.700	(0.200)	46.5	3.26	2.5%	---	---
35.0	34.71	2.93	3.37	(1.050)	1.848	(1.020)	0.670	0.695	(0.200)	37.9	4.06	2.5%	---	---
40.1$^{(*)}$	31.76	2.42	2.74	(1.050)	1.934	(1.020)	0.727	0.678	(0.200)	32.4	6.94	3.0%	9.12	±0.04
45.4	28.35	2.63	2.36	(1.050)	1.969	(1.020)	0.757	0.611	(0.200)	30.2	5.69	3.0%	---	---
49.5	26.82	1.69	1.88	(1.050)	1.841	(1.020)	0.825	0.630	(0.200)	18.6	2.63	10%	6.04	±0.06

(*) E_p = 38.7 MeV for the polarization data.

Note: The parameters in parenthesis were kept fixed during the search.

52.

smoothly with increasing energy, while the other parameters vary only slightly.

In order to further investigate the energy dependence of the potential an analysis was attempted keeping the geometrical parameters fixed to values independent of energy.

Three sets of averaged geometrical parameters were used. The first was obtained by averaging over the optimum parameters corresponding to all six energies and gave very poor fits in all cases. The second was obtained averaging over the parameters corresponding to the best fits at 25.9 and 29.9 MeV. The fits obtained with this geometry were good at the two lower energies but very poor at the energies above 30 MeV and the energy dependence of the dynamical parameters was irregular. Finally, a third geometry was extracted from the parameters corresponding to the second group of energies [*]. The dynamical parameters obtained with this geometry are shown in table 2, where the values of σ_{re}^{th}, χ_r^2/N_α, and χ_p^2/N_p are also given. On the basis of the values of χ_σ^2/N_σ and $\Delta\sigma$ the fit at 25.9 MeV can be considered quite acceptable. The position of the maxima of the experimental angular distribution is well reproduced by the calculations, which, however, give too small values for the cross-sections in the range $90°$ to $140°$ c.m. An improvement is apparent at 29.9 MeV and at 35.0 MeV the agreement between the theoretical and experimental differential cross-sections is good. At the higher

---

[*] It was found that a slight improvement of the fits was obtained by letting r_D assume a value larger than the average of the best fit parameters for the energies of the second group.

TABLE 2 - OPTICAL MODEL PARAMETERS WITH FIXED GEOMETRY

r_o = 1.050 fm r_D = 1.923 fm. r_s = 1.020 fm

a = 0.745 fm a_D = 0.654 fm a_s = 0.200 fm

E_p (MeV)	V (MeV)	W_D (MeV)	V_s (MeV)	σ_{re}^{th} (fm^2)	χ_σ^2/N_σ	Δ_σ	χ_p^2/N_p	Δp
25.9	37.17	2.44	4.07	37.5	23.5	3.5%	---	---
29.9	35.25	2.30	3.08	33.7	28.9	2.5%	---	---
35.0	34.32	2.42	3.03	32.8	24.6	2.5%	---	---
40.1$^{(*)}$	32.08	2.54	2.92	32.2	8.94	3.0%	10.3	±0.04
45.4	30.13	3.11	2.53	35.8	8.07	3.0%	---	---
49.5	25.33	1.49	1.48	18.6	3.48	10%	15.6	±0.06

(*) E_p=38.7 MeV for the polarization data.

energies the fits for the differential cross-sections are good and

those for the polarizations reasonable.

From the analysis with fixed geometry one can derive the follow-

ing averaged potential:

$$r_o = 1.050 \text{ fm} \qquad r_D = 1.923 \text{ fm} \qquad r_S = 1.020 \text{ fm}$$
$$a = 0.745 \text{ fm} \qquad a_D = 0.654 \text{ fm} \qquad a_S = 0.200 \text{ fm}$$
$$V = 46.2 \text{ MeV}-0.35E_p \qquad W_D = 2.38 \text{ MeV} \qquad V_S = 2.85 \text{ MeV}$$

It may be observed that the energy dependence of the real central potential

is in agreement with that found for medium weight nuclei.

In conclusion the analysis with fixed geometry gives acceptable

fits with reasonable values of the parameters over the whole energy range

considered. The quality of the fits at the lower energies can be dramati-

cally improved if one lets the parameters acquire values markedly different

from those at energies greater than 30 MeV. A possible explanation for

the anomalous energy behaviour may perhaps be found in the following argument.

As has been already mentioned [*], it is quite possible that the

elastic channel is strongly coupled to the inelastic channel corresponding

to scattering from the 2.184 MeV level. It is known [**] that in the case

of strong coupling the parameters obtained from the simple optical model

may be different from those obtained from a generalized optical model and

that the difference increases with the decreasing energy. If the hypothesis

of strong coupling is correct and one assumes that a generalized optical model

---

(*) see chapter 1. section 4

(**) see Buck {30}.

would give parameters which vary regularly with energy, then it is
quite possible that at energies above 30 MeV the simple optical model
gives parameters very close to those that would be obtained from the
generalized optical model, while at the lower energies the difference
due to the coupling becomes apparent. The irregular energy dependence
of the potential could also be explained by the effect of resonances in
the compound system ^{7}Be, as in the case of p + ^{12}C {24},and p + ^{16}O
{44-47} elastic scattering between 20 and 30 MeV.

While further studies are necessary to clarify this point,
the quality of the fits obtained indicates that the optical model
applies to ^{6}Li better perhaps than one would expect for such a light
nucleus.

3-2. Results and Discussion (inelastic scattering)

Tables of the differential cross-sections obtained for the scat-
tering from the first excited state (3^+, T=0, 2.184 MeV) are given in
appendix II. The angular distributions for the scattering from this
level are shown in Fig. 9. The dimensions of the error bars would be
comparable to the size of the experimental points. The curves show little
structure and the variation with energy is smooth.

Tabulated values for the scattering from the (0^+, T=1, 3.562 MeV)
second excited state at 25.9 MeV incident energy are also given in appen-
dix II. In Fig. 10 the differential cross-sections obtained in the pre-
sent experiment are shown together with the experimental data of Austin
and Crawley {34}. As has been discussed in sections 1 - 4, an analysis

of the data for inelastic scattering from the second excited state in terms of a microscopic theory may yield information on the strength of the spin-isospin dependent effective interaction. The curve shown in Fig. 10 represents the results of the calculations done by Austin and Crawley with a spin-isospin dependent potential of Yukawa shape. The two sets of experimental results are consistent. The agreement between theory and experiment is good only at forward angles, and is obtained for a spin-isospin dependent interaction which has a strength of 12.7 MeV and a range of 1 fm.

The reduction of the data for the scattering from the second excited state at 45.4 MeV is in progress. An analysis of these data will give information on the energy dependence of the spin-isospin dependent effective potential, which other investigations {35,36} indicate to be nearly constant over the energy range 30-50 MeV.

^{6}Li (p,p) ^{6}Li (2.184 MeV 3$^+$)

25.9 MeV

29.9 MeV

30.0 MeV

40.1 MeV

45.4 MeV

$d\sigma/d\Omega$ in mb/sr

$\Theta_{c.m.}$ in DEGREES
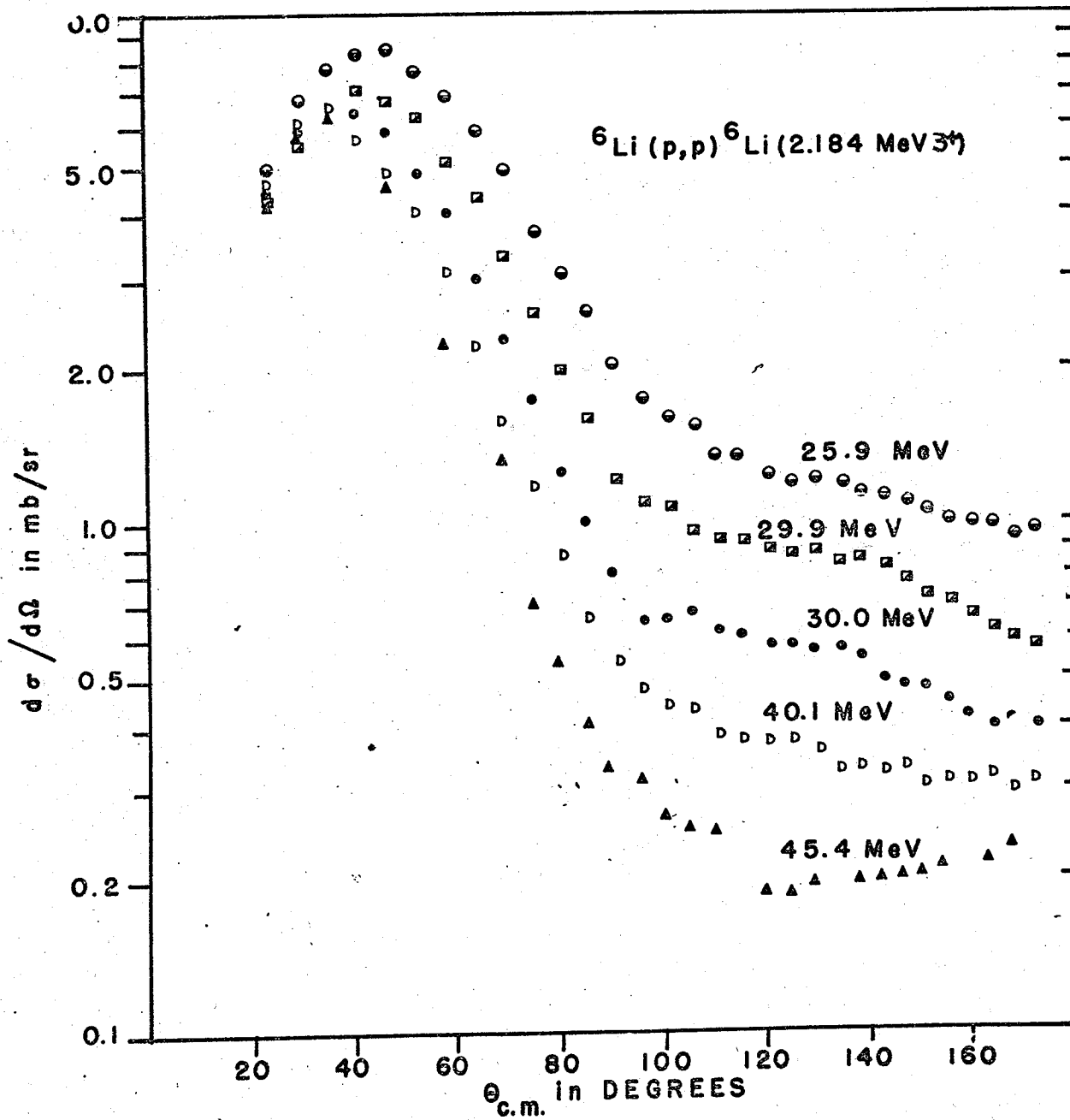
Fig. 9
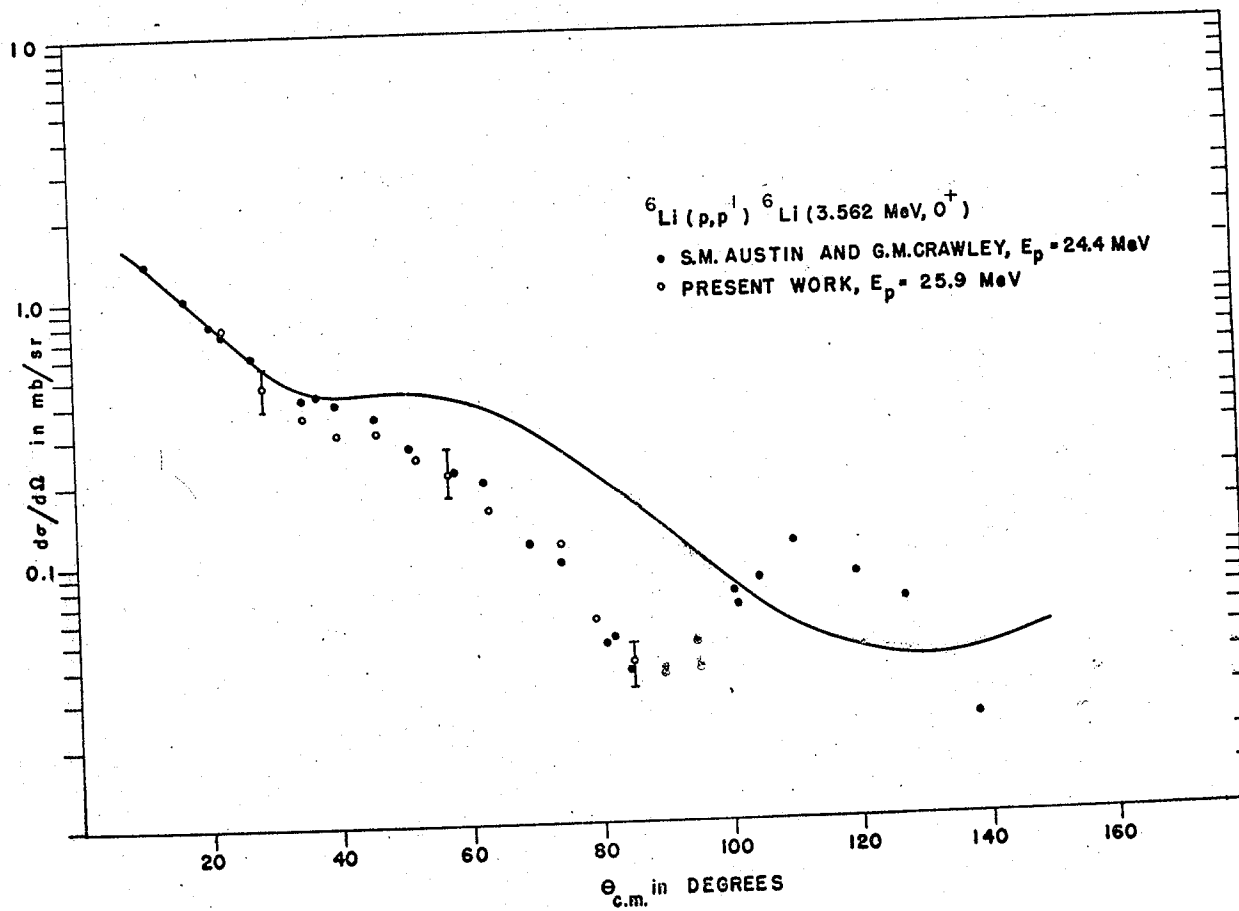
Fig. 10

APPENDIX I

Derivation of some Formulas Used in the Reduction of the Data

The differential cross-section for the scattering of an incident beam of particles by a single scattering center is a function of the scattering angle θ which is defined by:

$$\text{(a)} \qquad \frac{d\sigma}{d\Omega} = \frac{n(\theta)}{I_0} \qquad ,$$

where $n(\theta)$ is the number of particles scattered per unit time in the unit solid angle about θ and I_0 is the incident flux. If Y is the number of protons scattered by n_t target atoms in the solid angle $\Delta\Omega$ during the time Δt, then

$$\text{(b)} \qquad n(\theta) = \frac{Y}{n_t \Delta\Omega\Delta t} \ .$$

The incident flux of protons is related to total charge Q carried by the beam in a time Δt by

$$\text{(c)} \quad I_0 = \frac{Q}{eS\Delta t}$$

where S is the area of target (*) and e is the electronic charge.

If the target is made of a spearated isotope of mass number A, the number of atoms in the target can be expressed as the product of the Avogadro number N times the ratio of the mass of the target M to the mass of one mole

$$\text{(d)} \qquad n_t = \frac{M}{A} N \qquad ,$$

(*) Here and in the following it is assumed that the entire surface of the target is exposed to the beam. The derivations given, however, maintain their validity in the general case, provided that one refers the quantities M, S and n_t to the portion of the target crossed by the beam.

where M is in grams. By substituting (b), (c), and (d) into (a) one

obtains

$$\text{(e)} \quad \frac{d\sigma}{d\Omega} = \frac{eA}{N} \ \frac{Y}{\frac{QM\Delta\Omega}{S}} \quad .$$

The ratio M/S is the measured target thickness t. If one wants

to express t in the usual units mg/cm^2 and Q in nC, then

$$\frac{eA}{N} = (2.66018 \times 10^{-31} A)nC \times mg.$$

hence, converting from cm^2 to mb:

$$\text{(f)} \quad \frac{d\sigma}{d\Omega} = 2.66018 \times 10^{-4} \ \frac{AY}{Qt\Delta\Omega} \quad mb/s{\cdot}r.$$

which becomes identical to equation (16) of chapter 2 if one

introduces the dead time correction factor τ.

Suppose now that the target is not isotopically pure but con-

tains n_1 and n_2 atoms of the isotopes of atomic numbers A_1 and A_2

respectively with

$$n_1 + n_2 = n_t \quad , \quad \frac{n_1}{n_t} = \alpha.$$

Equation (d) still holds, but A must now be interpreted as the atomic

weight of the mixture of the two isotopes, that is, A grams is the

mass of N atoms of which αN have atomic number A, and $(1-\alpha)N$ have

atomic number A_2:

$$\text{(g)} \quad A = \alpha A_1 + (1-\alpha)A_2$$

The differential cross-section for scattering by the isotope A,

is obtained substituting in (a) the expression (c) for I_0 and for

$n(\theta)$ an expression analagous to (b), but containing n_1 instead of

n_t:

$$\text{(h)} \quad \frac{d\sigma}{d\Omega} = \frac{e}{n_1} \frac{Y}{Q\frac{1}{S}\Delta\Omega}$$

From the definition of α and from (g) it follows

$$n_1 = \alpha n_t = \alpha\frac{M}{A}N = \frac{M}{A_1 + \frac{1-\alpha}{\alpha}A_2} N$$

Inserting this expression for n_1 in (h) one obtains an expression

which differs from (e) only in the substitution of A with the quantity

$$\mathcal{A} = A_1 + \frac{1-\alpha}{\alpha}A_2$$

in agreement with equation (17) of Chapter 2.

Finally, consider a target containing n atoms of the isotope A,

and n_i atoms of an impurity A_i. The correct differential cross-section

for scattering by the isotope A is given by:

$$\frac{d\sigma}{d\Omega} = \frac{e\ Y}{Q\frac{n}{S}\Delta\Omega}$$

The measured target thickness, however, contains a contribution from

the impurity A_1:

$$t = \frac{nA + n_iA_i}{NS} \quad .$$

Solving for n/S and substituting in the previous equation one obtains

the differential cross-section for scattering from the isotope A in terms

of the measured target thickness and of the number of atoms and

atomic number of the impurity:

$$(g) \quad \frac{d\sigma}{d\Omega} = \frac{eA}{N} \; \frac{Y}{Q(t-\frac{n_i A_i}{NS})\Delta\Omega}$$

It is quite natural to call the quantity $\frac{n_i A_i}{NS}$ the "target thickness

for the impurity" as in equation (18) of chapter 2. It should be

noted however, that the derivation does not depend on a model in which

the impurity atoms are localized in a layer of area S and thickness

t.

Considering the differential cross-section for scattering by

the impurity at an angle at which the corresponding peak is completely

resolved:

$$\frac{d\sigma}{d\Omega})_i = \frac{e \, A_i}{N} \; \frac{Y_i}{Q \, t_i \Delta\Omega} \quad ,$$

the value of $t_i = \frac{n_i A_i}{NS}$ can be derived from a known value of $\frac{d\sigma}{d\Omega})_i$

and measured values of Y_i, Q, and $\Delta\Omega$.

APPENDIX II

TABLES OF DIFFERENTIAL CROSS-SECTIONS

^{6}Li(p,p) ^{6}Li(g.s.) $\underline{E_p = 25.9 \pm 0.2 \text{ MeV}}$

θ_{lab} [deg]	$d\sigma/d\Omega)_{lab}$ [mb./s.r.]	θ_{cm} [deg]	$d\sigma/d\Omega)_{cm}$ [mb./s.r.]	rel. error [%]
19.8	368.0	23.2	273.3	2.4
24.8	284.5	28.9	213.5	1.7
29.8	187.1	34.7	142.2	2.1
34.8	119.0	40.4	91.8	2.4
39.8	72.0	46.1	56.5	2.8
44.8	40.2	51.8	32.2	3.4
49.8	24.24	57.3	19.80	3.6
54.8	11.32	62.9	9.46	4.4
59.8	6.16	68.3	5.27	3.7
64.8	3.75	73.7	3.30	4.5
69.8	2.93	79.1	2.65	4.0
74.8	2.75	84.3	2.56	3.9
79.8	2.67	89.5	2.55	3.1
84.8	2.54	94.6	2.50	3.6
89.8	2.488	99.7	2.52	4.0
94.8	2.367	104.6	2.475	3.6
99.8	2.069	109.5	2.230	3.5
104.8	1.783	114.3	1.981	4.0
109.8	1.446	119.1	1.654	4.9
114.8	1.149	123.7	1.352	4.5
119.8	0.899	128.3	1.087	3.8
124.8	0.681	132.9	0.847	3.7
129.8	0.519	137.3	0.662	3.2
134.8	0.409	141.8	0.534	3.2
139.8	0.322	146.1	0.429	2.6
144.8	0.274	150.5	0.373	2.9
149.8	0.247	154.7	0.342	3.1
154.8	0.234	159.0	0.329	3.2
159.8	0.234	163.2	0.332	3.2
164.8	0.241	167.4	0.346	3.1
169.8	0.247	171.5	0.358	3.0

^{6}Li(p,p) ^{6}Li(g.s.)   Ep = 29.9 ± 0.2 MeV

θ_{lab} [deg]	$d\sigma/d\Omega)_{lab}$ [mb/s.r.]	θ_{cm} [deg]	$d\sigma/d\Omega)_{cm}$ [mb/s.r.]	rel.error [%]
20.0	323.9	23.4	240.4	1.5
25.0	229.6	29.2	172.2	1.4
30.0	150.4	34.9	114.3	1.6
35.0	90.4	40.7	69.8	2.0
40.0	50.42	46.3	39.57	1.9
45.0	26.64	52.0	21.31	2.0
50.0	13.42	57.6	10.97	2.2
55.0	6.88	63.1	5.75	2.2
60.0	3.709	68.5	3.177	2.4
65.0	2.510	73.9	2.206	2.2
70.0	2.027	79.3	1.831	2.5
75.0	1.825	84.5	1.696	2.5
80.0	1.699	89.7	1.625	2.3
85.0	1.554	94.8	1.532	2.9
90.0	1.453	99.9	1.475	2.5
95.0	1.257	104.8	1.316	3.0
100.0	1.027	109.7	1.109	3.7
105.0	0.836	114.5	0.930	3.5
110.0	0.664	119.3	0.761	3.6
115.0	0.512	123.9	0.604	3.8
120.0	0.402	128.5	0.488	3.5
125.0	0.3140	133.1	0.391	2.8
130.0	0.2567	137.5	0.3276	2.2
135.0	0.2038	141.9	0.2662	2.8
140.0	0.1733	146.3	0.2313	2.2
145.0	0.1576	150.6	0.2145	2.4
150.0	0.1376	154.9	0.1904	2.7
155.0	0.1304	159.1	0.1832	2.0
160.0	0.1321	163.3	0.1879	1.9
165.0	0.1281	167.5	0.1839	2.1
170.0	0.1589	171.7	0.2298	2.0

^{6}Li(p,p) ^{6}Li(g.s.)   Ep = 35.0 ± 0.2 MeV

θ_{lab} [deg]	dσ/dΩ)$_{lab}$ [mb/s.r.]	θ_{cm} [deg]	dσ/dΩ)$_{cm}$ [mb/s.r.]	rel. error [%]
20.0	272.1	23.4	201.7	2.8
25.0	193.0	29.2	144.6	1.4
30.0	118.7	35.0	90.1	1.8
35.0	67.2	40.7	51.8	2.1
40.0	35.49	46.4	27.83	2.3
45.0	17.07	52.0	13.65	2.9
50.0	8.01	57.6	6.54	2.9
55.0	3.93	63.1	3.28	3.6
60.0	2.368	68.6	2.028	2.4
65.0	1.684	74.0	1.480	2.3
70.0	1.428	79.3	1.290	1.9
75.0	1.273	84.6	1.183	2.1
80.0	1.076	89.8	1.029	2.4
85.0	0.910	94.9	0.897	2.8
90.0	0.781	99.9	0.794	2.9
95.0	0.622	104.9	0.651	2.8
100.0	0.456	109.7	0.493	3.1
105.0	0.344	114.5	0.383	3.2
110.0	0.2607	119.3	0.2988	3.2
115.0	0.2078	123.9	0.2452	3.0
120.0	0.1698	128.5	0.2060	2.6
125.0	0.1456	133.1	0.1814	2.4
130.0	0.1299	137.5	0.1659	2.2
135.0	0.1122	142.0	0.1467	2.1
140.0	0.1055	146.3	0.1410	1.8
144.1	0.0995	149.9	0.1350	1.6
150.0	0.0890	154.9	0.1234	1.7
155.0	0.0813	159.2	0.1143	1.8
160.0	0.0770	163.4	0.1096	1.9
165.0	0.0692	167.5	0.0995	2.1
170.0	0.0673	171.7	0.0974	2.2

^{6}Li(p,p) ^{6}Li(g.s.) E_p = 40.1 ± 0.2 MeV

θ_{lab} [deg]	$d\sigma/d\Omega)_{lab}$ [mb/s.r.]	θ_{cm} [deg]	$d\sigma/d\Omega)_{cm}$ [mb/s.r.]	rel.error [%]
20.0	243.8	23.4	180.5	1.6
25.0	158.4	29.2	118.5	1.7
30.0	90.0	35.0	68.2	2.2
35.0	48.4	40.7	37.24	2.6
40.0	22.63	46.4	17.73	2.7
45.0	10.20	52.0	8.14	4.6
50.0	4.77	57.6	3.89	3.3
55.0	2.307	63.2	1.926	3.6
60.0	1.541	68.6	1.318	2.5
65.0	1.224	74.0	1.075	2.2
70.0	1.036	79.4	0.935	1.9
75.0	0.895	84.6	0.831	1.8
80.0	0.724	89.8	0.693	1.7
85.0	0.555	94.9	0.547	2.3
90.0	0.414	99.9	0.420	3.2
95.0	0.294	104.9	0.308	3.4
100.0	0.2016	109.8	0.2178	3.4
105.0	0.1449	114.6	0.1613	3.6
110.0	0.1082	119.3	0.1241	3.3
115.0	0.0925	124.0	0.1092	3.3
120.0	0.0831	128.6	0.1009	2.9
125.0	0.0771	133.1	0.0962	2.9
130.0	0.0743	137.6	0.0950	2.8
135.0	0.0697	142.0	0.0912	3.3
140.0	0.0680	146.3	0.0910	3.2
145.0	0.0655	150.7	0.0893	2.9
150.0	0.0594	154.9	0.0824	3.1
155.0	0.0512	159.2	0.0721	3.1
160.0	0.0468	163.4	0.0667	3.2
165.0	0.0408	167.5	0.0588	3.5
170.0	0.0353	171.7	0.0512	4.0

^{6}Li(p,p) ^{6}Li(g.s.)   Ep = 45.4 ± 0.2 MeV

θ_{lab} [deg]	$d\sigma/d\Omega)_{lab}$ [mb/s.r.]	θ_{cm} [deg]	$d\sigma/d\Omega)_{cm}$ [mb/s.r.]	rel.error [%]
19.8	176.3	23.2	130.3	3.4
24.8	107.1	29.0	80.0	3.9
29.8	62.3	34.8	47.1	2.8
34.8	31.03	40.5	23.85	3.2
39.8	13.50	46.2	10.55	3.2
44.8	5.59	51.8	4.46	4.4
49.8	2.411	57.4	1.964	3.8
54.8	1.135	63.0	0.946	4.5
59.8	0.887	68.4	0.758	2.5
64.8	0.762	73.8	0.669	2.3
69.8	0.675	79.2	0.609	2.3
74.8	0.551	84.4	0.511	2.5
79.8	0.414	89.6	0.396	3.1
84.8	0.2952	94.7	0.2907	3.0
89.8	0.2010	99.8	0.2040	2.8
94.8	0.1355	104.7	0.1418	3.1
99.8	0.0936	109.6	0.1011	3.5
109.8	0.0439	119.2	0.0503	4.6
114.8	0.0417	123.8	0.0492	3.5
119.8	0.0437	128.4	0.0530	2.5
124.8	0.0466	133.0	0.0581	2.7
129.8	0.0461	137.4	0.0590	3.0
134.8	0.0454	141.8	0.0594	2.9
139.8	0.0419	146.2	0.0560	3.1
144.8	0.0378	150.5	0.0516	3.2
149.8	0.0347	154.8	0.0482	3.4
154.8	0.0299	159.0	0.0421	3.6
159.8	0.0278	163.2	0.0396	3.6
164.8	0.0278	167.4	0.0401	3.6

^{6}Li(p,p!)^{6}Li *(2.184 MeV level)   Ep = 25.9 ± 0.2 MeV

θ_{lab} [deg]	dσ/dΩ)$_{lab}$ [mb./s.r.]	θ_{cm} [deg]	dσ/dΩ)$_{cm}$ [mb./s.r.]	rel.error [%]
19.8	6.76	23.3	4.95	2.5
24.8	9.13	29.1	6.76	1.9
29.8	10.32	34.9	7.74	1.9
34.8	10.95	40.7	8.35	1.9
39.8	10.91	46.4	8.46	1.7
44.8	9.70	52.1	7.68	2.2
49.8	8.59	57.7	6.95	3.1
54.8	7.17	63.3	5.94	3.0
59.8	5.82	68.7	4.95	2.8
64.8	4.30	74.2	3.75	3.0
69.8	3.51	79.5	3.154	3.1
74.8	2.846	84.8	2.634	3.3
79.8	2.195	90.0	2.094	3.2
84.8	1.815	95.1	1.786	3.4
89.8	1.644	100.1	1.670	4.6
94.8	1.523	105.1	1.597	3.0
99.8	1.290	110.0	1.397	3.0
104.8	1.228	114.8	1.373	2.8
109.8	1.093	119.5	1.260	2.7
114.8	1.044	124.2	1.240	2.5
119.8	1.017	128.8	1.245	2.2
124.8	0.973	133.3	1.224	2.1
129.8	0.907	137.7	1.172	2.1
134.8	0.879	142.1	1.164	2.0
139.8	0.847	146.4	1.148	2.0
144.8	0.788	150.7	1.089	1.9
149.8	0.744	155.0	1.048	1.9
154.8	0.724	159.2	1.035	1.9
159.8	0.699	163.3	1.012	1.9
164.8	0.665	167.5	0.973	2.0
169.8	0.676	171.6	0.998	1.9

^{6}Li(p,p') ^{6}Li *(2.184 MeV level)   Ep = 29.9 ± 0.2 MeV

θ_{lab} [deg]	$d\sigma/d\Omega)_{lab}$ [mb./s.r.]	θ_{cm} [deg]	$d\sigma/d\Omega)_{cm}$ [mb./s.r.]	rel.error [%]
20.0	5.97	23.5	4.37	3.0
25.0	7.67	29.4	5.69	2.6
30.0	8.81	35.1	6.62	2.5
35.0	9.26	40.9	7.06	1.2
40.0	8.64	46.6	6.71	2.4
45.0	7.92	52.3	6.28	2.1
50.0	6.30	57.9	5.10	2.3
55.0	5.30	63.4	4.40	2.5
60.0	3.99	68.9	3.398	2.6
65.0	3.002	74.3	2.626	2.9
70.0	2.237	79.7	2.013	3.0
75.0	1.753	85.0	1.625	2.6
80.0	1.292	90.2	1.234	2.7
85.0	1.128	95.3	1.112	2.8
90.0	1.074	100.3	1.092	1.9
95.0	0.919	105.3	0.965	1.9
100.0	0.863	110.1	0.936	1.8
105.0	0.840	114.9	0.939	1.8
110.0	0.779	119.7	0.898	1.8
115.0	0.738	124.3	0.878	1.6
120.0	0.725	128.9	0.887	1.8
125.0	0.674	133.4	0.848	1.8
130.0	0.663	137.9	0.856	1.7
135.0	0.627	142.2	0.830	1.8
140.0	0.574	146.6	0.778	1.7
145.0	0.526	150.9	0.727	1.8
150.0	0.4992	155.1	0.702	1.9
155.0	0.4646	159.3	0.664	1.9
160.0	0.4349	163.5	0.629	2.0
165.0	0.4040	167.6	0.591	2.1
170.0	0.3905	171.8	0.575	2.1

^{6}Li(p,p') ^{6}Li *(2.184 MeV level)   Ep = 35.0 ± 0.2 MeV

θ_{lab} [deg]	dσ/ dΩ)$_{lab}$ [mb./s.r.]	θ_{cm} [deg]	dσ/dΩ)$_{cm}$ [mb./s.r.]	rel.error [%]
20.0	6.09	23.5	4.468	2.0
25.0	7.90	29.3	5.86	2.1
30.0	8.49	35.1	6.38	1.7
35.0	8.37	40.9	6.39	2.5
40.0	7.56	46.6	5.883	1.5
45.0	6.16	52.3	4.888	1.7
50.0	4.977	57.9	4.036	1.8
55.0	3.657	63.4	3.037	2.1
60.0	2.703	68.9	2.302	2.2
65.0	2.017	74.3	1.765	2.4
70.0	1.431	79.7	1.288	2.6
75.0	1.105	84.9	1.024	2.8
80.0	0.849	90.1	0.811	3.1
85.0	0.669	95.2	0.659	3.2
90.0	0.647	100.3	0.658	2.8
95.0	0.642	105.2	0.674	2.6
100.0	0.576	110.1	0.624	3.4
105.0	0.546	114.9	0.610	2.2
110.0	0.504	119.6	0.581	4.2
115.0	0.492	124.3	0.584	4.0
120.0	0.470	128.9	0.575	2.4
125.0	0.4564	133.4	0.5738	1.5
130.0	0.433	137.8	0.558	2.7
135.0	0.3889	142.2	0.5142	1.6
140.0	0.3691	146.6	0.4991	1.8
144.1	0.3510	150.1	0.4827	1.6
150.0	0.3240	155.1	0.4551	1.6
155.0	0.3007	159.3	0.4290	2.1
160.0	0.2835	163.5	0.4096	1.8
165.0	0.285	167.6	0.416	7.6
170.0	0.2771	171.8	0.407	3.0

$^6Li(p,p')$ ^6Li *(2.184 MeV level)   Ep = 40.1 ± 0.2 MeV

θ_{lab} [deg]	$d\sigma/d\Omega)_{lab}$ [mb./s.r.]	θ_{cm} [deg]	$d\sigma/d\Omega)_{cm}$ [mb./s.r.]	rel. error [%]
20.0	6.27	23.5	4.60	2.5
25.0	8.13	29.3	6.03	1.9
30.0	8.60	35.1	6.47	1.7
35.0	7.44	40.9	5.69	2.0
40.0	6.23	46.6	4.85	2.2
45.0	5.162	52.3	4.096	1.6
50.0	3.843	57.9	3.117	2.1
55.0	2.651	63.4	2.202	2.7
60.0	1.885	68.9	1.606	2.9
65.0	1.360	74.3	1.190	2.9
70.0	0.969	79.7	0.873	2.7
75.0	0.718	84.9	0.666	3.1
80.0	0.567	90.1	0.542	3.3
85.0	0.492	95.2	0.485	2.9
90.0	0.438	100.3	0.445	2.8
95.0	0.411	105.2	0.432	2.5
100.0	0.3602	110.1	0.3903	2.2
105.0	0.3392	114.9	0.3792	2.2
110.0	0.3254	119.6	0.3751	2.1
115.0	0.319	124.3	0.379	3.3
120.0	0.2986	128.9	0.3651	2.0
125.0	0.2642	133.4	0.3321	2.0
130.0	0.2578	137.8	0.3326	2.0
135.0	0.2502	142.2	0.3307	2.2
140.0	0.2488	146.6	0.3363	1.9
145.0	0.2233	150.8	0.3079	2.1
150.0	0.2278	155.1	0.3198	2.1
155.0	0.2236	159.3	0.3188	2.0
160.0	0.2224	163.5	0.3211	2.0
165.0	0.2114	167.6	0.3084	2.0
170.0	0.2171	171.8	0.3190	2.0

^{6}Li(p,p') ^{6}Li *(2.184 MeV level)   Ep = 45.4 $\pm$ 0.2 MeV

θ_{lab} [deg]	$d\sigma/d\Omega)_{lab}$ [mb./s.r.]	θ_{cm} [deg]	$d\sigma/d\Omega)_{cm}$ [mb./s.r.]	rel. error [%]
20.0	5.70	23.5	4.18	3.7
25.0	7.79	29.3	5.78	4.1
30.0	8.46	35.1	6.36	3.0
40.0	5.88	46.6	4.57	3.4
50.0	2.778	57.9	2.253	4.1
60.0	1.542	68.9	1.314	3.2
64.8	0.798	74.1	0.697	2.4
69.8	0.585	79.4	0.526	2.4
74.8	0.440	84.7	0.408	2.5
79.8	0.3509	89.9	0.3349	2.4
84.8	0.3164	95.0	0.3116	2.1
89.8	0.2651	100.1	0.2693	2.1
94.8	0.2404	105.0	0.2521	2.0
99.8	0.2274	109.9	0.2461	1.8
109.8	0.1622	119.4	0.1867	1.8
114.8	0.1568	124.1	0.1861	1.8
119.8	0.1630	128.7	0.1991	2.1
129.8	0.1584	137.6	0.2041	1.9
134.8	0.1511	142.0	0.1995	2.0
139.8	0.1482	146.4	0.2001	2.0
144.8	0.1499	150.7	0.2066	2.0
149.8	0.1503	154.9	0.2108	2.0
159.8	0.1521	163.3	0.2194	2.0
164.8	0.1618	167.5	0.2358	1.9

^{6}Li(p,p') ^{6}Li *(3.562 MeV level)   Ep = 25.9 ± 0.2 MeV

θ_{lab} [deg]	$d\sigma/d\Omega)_{lab}$ [mb./s.r.]	θ_{cm} [deg]	$d\sigma/d\Omega)_{cm}$ [mb./s.r.]	
19.8	1.06	23.4	0.76	
24.8	0.63	29.3	0.465	
29.8	0.479	35.1	0.356	
34.8	0.403	40.9	0.304	typical
39.8	0.401	46.7	0.308	relative error ≈ 20%
44.8	0.317	52.4	0.249	
49.8	0.271	58.0	0.218	
54.8	0.186	63.6	0.154	
64.8	0.131	74.5	0.114	
69.8	0.065	79.9	0.059	
74.8	0.434	85.2	0.0401	
84.8	0.0387	95.5	0.0381	

REFERENCES

{1.} P. E. Hodgson, "The Optical Model of Elastic Scattering" Oxford, 1963.

{2.} P. B. Jones, "The Optical Model in Nuclear and Particle Physics", Interscience, 1963.

{3.} G. Breit and E. P. Wigner, Phys. Rev. $\underline{49}$ (1936) 519.

{4.} R. M. Eisberg and G. Igo, Phys. Rev. $\underline{93}$ (1954) 1039.

{5.} H. H. Barshall, Phys. Rev. $\underline{79}$ (1950) 745.

{6.} H. Feshbach, C. E. Porter and V. F. Weisskopf, Phys. Rev. $\underline{96}$ (1954) 488.

{7.} R. D. Woods and D. S. Saxon, Phys. Rev. $\underline{95}$ (1954) 577.

{8.} D. Kurath, Phys. Rev. $\underline{88}$ (1952) 804

{9.} E. Feenberg and E. Wigner, Phys. Rev. $\underline{51}$ (1937) 95

{10.} E. Feenberg and M. Phyllips, Phys. Rev. $\underline{51}$ (1937) 597.

{11.} D. R. Inglis, Phys. Rev. $\underline{87}$ (1952) 915.

{12.} D. R. Inglis, Rev. Modern Phys. $\underline{25}$ (1953) 390.

{13.} D. Kurath, Phys. Rev. $\underline{101}$ (1956) 216.

{14.} Y. C. Tang, K. Windermuth and L. D. Pearlstein, Phys. Rev. $\underline{123}$ (1961) 548.

{15.} K. Wildermuth and W. McLure, "Cluster Representation of Nuclei", Springer-Verlag 1966.

{16.} F. G. Perey, Phys. Rev. $\underline{131}$ (1963) 745.

{17.} L. Rosen, J. G. Beery, A. S. Goldhaber and E. H. Auerback, Ann. Phys. $\underline{34}$ (1965) 96.

{18.} M. P. Fricke, E. E. Gross, B. J. Morton and A. Zucker, Phys. Rev. $\underline{156}$ (1967) 1207.

{19.} P. E. Hodgson, Phys. Rev. Letters $\underline{6}$ (1961) 358.

{20.} A. Johanson, U. Svanberg and P. E. Hodgson, Arkiv. Fysik $\underline{19}$ (1961) 358.

{21.} M. P. Fricke and G. R. Satchler, Phys. Rev. $\underline{139B}$ (1965) 567.

{22.} J. K. Dickens, D. A. Haner and C. N. Waddel, Phys. Rev. <u>129</u> (1963) 743.

{23.} J. K. Dickens, D. A. Haner and C. N. Waddel, Phys. Rev. <u>132</u> (1963) 2159.

{24.} R. M. Craig, J. C. Dore, G. W. Greenlees, J. Lowe and D. L. Watson, Nucl. Phys. <u>83</u> (1966) 493.

{25.} J. A. Fannon, E. J. Burge and D. A. Smith, Nucl. Phys. <u>83</u> (1967) 263.

{26.} W. T. H. van Oers and J. M. Cameron, Phys. Rev. <u>184</u> (1969) 1061.

{27.} R. K. Cole, C. N. Waddell, R. R. Dittman and H. S. Sandher, Nucl. Phys. <u>75</u> (1966) 241.

{28.} F. G. Perey, USAEC Doc. ANL-6848 (1964) 114.

{29.} D. M. Chase, L. Wilets and A. R. Edmonds, Phys. Rev. <u>110</u> (1958) 1080.

{30.} B. Buck, Phys. Rev. <u>130</u> (1963) 712.

{31.} T. Tamura, Rev. Modern Phys. <u>37</u> (1965)

{32.} V. A. Madsen, Nucl. Phys. <u>80</u> (1966) 177.

{33.} G. R. Satchler, Nucl. Phys. <u>77</u> (1966) 481.

{34.} S. M. Austin and G. M. Crawley, Phys. Letters <u>27B</u> (1968) 570.

{35.} S. M. Austin, P. J. Locard, W. Benson and G. M. Crawley, Phys. Rev. <u>176</u> (1968) 1227.

{36.} A. S. Clough, C. J. Batty, B. E. Bonner, C. Tschalar and L. E. Williams, Nucl. Phys. <u>A137</u> (1969) 222.

{37.} J. J. Burgerjon, Nucl. Inst. Meth. <u>43</u> (1966) 381.

{38.} R. Smythe, Rev. Sci. Instr. <u>35</u> (1964) 1197.

{39.} F. S. Goulding, D. A. Landis, J. Cerny and R. H. Pehl, Nucl. Instr. <u>31</u> (1964) 1.

{40.} C. F. Hwang, G. Clausnitzer, D. H. Nordby, S. Suwa and J. H. Williams, Phys. Rev. <u>131</u> (1963) 2602.

{41.} G. S. Mani, A. B. Dix and D. Jones, PLA Progress Report (1967) unpublished.

{42.} M. A. Melkanoff, J. Raynal and T. Sawada, UCLA report no. 66-10 (unpublished).

{43.} S. W. Chen and N. M. Hintz, "Nuclear Forces and the Few Nucleon Problem" (proc. int. conf., London 1959) p. 683.

{44.} O. Karban, P. D. Greaves, V. Hnizdo, J. Lowe, N. Beronic, H. Wojciechowski and G. W. Greenlees, Nucl. Phys. A 132 (1969) 529.

{45.} H. Appel, S. N. Bunker, J. M. Cameron, M. B. Epstein, J. R. Quinn, J. R. Richardson, and J. W. Verba, Bull. Am. Phys. Soc. 13 (1968) 680.

{46.} S. N. Bunker, H. Appel, J. M. Cameron, M. B. Epstein, J. R. Quinn, J. R. Richardson and J. W. Verba, Bull. Am. Phys. Soc. 14 (1969) 529.

{47.} S. N. Bunker, Ph. D. Thesis, U.C.L.A. (1970) unpublished.